Radar Aided INS Navigation Filter with Magnetometer Based Attitude Measurements

by

John Williams

A thesis submitted to the Graduate Faculty of
Auburn University
in partial fulfillment of the
requirements for the Degree of
Master of Science

Auburn, Alabama
December 15, 2018

Keywords: Magnetometer, Attitude Determination, Kalman Filter, Navigation

Approved by

David Bevly, Chair, Professor of Mechanical Engineering
Scott Martin, Professor of Mechanical Engineering
Lloyd Riggs, Professor of Electrical and Computer Engineering

Abstract

This thesis presents a method for GPS-free navigation using a radar-aided inertial navigation filter with a magnetometer based attitude measurement. GPS has become the popular tool of choice when considering navigation solutions today, however, GPS is a low-power signal that can be easily blocked by large structures or jamming. Previous work has been done on attitude and heading reference systems which use magnetometers and accelerometers to determine the attitude of a vehicle. The magnetometer and accelerometer attitude measurement can be incorporated into the measurement update of an Extended Kalman Filter (EKF). The EKF presented in this thesis propagates the inertial navigation solution in the time update, while the measurement update uses the radar and attitude measurements to correct the inertial navigation system propagation errors.

In this thesis, magnetometer calibration will first be discussed. A magnetometer calibration routine will be selected then verified though simulated and experimental tests. Then, an attitude determination algorithm that uses magnetometer and accelerometer measurements will be reviewed and tested in simulation and with experimental data. Next, intertial navigation system propagation errors will be discussed and how radar-aiding in an Extended Kalman Filter can reduce propagation errors. Radar target determination is overviewed next, and finally, a new filter called the Radar-Aided INS (RAINS) filter is proposed and tested in simulation. The results of RAINS filter analysis show the possibility of navigation completely independent of GPS. The radar used in this thesis is a Delphi Electronically Scanning Radar which provides measurements of range, range rate, and azimuth.

Acknowledgments

First and foremost I would like to thank Jesus Christ. His sacrifice on my behalf is a debt I could never hope repay, so it's the least I can do to live my life according to His will and to give Him all the honor and glory. He was my constant source of strength and peace, without Whom I would never have made it this far.

I would like to thank my parents for always supporting me in everything I do and providing for me so that I could pursue my dreams. Their constant love and support throughout my undergraduate and graduate career kept me sane and encouraged. I also want to thank my brother for being a role model for me in everything he does. Even now, I'm continuing in his footsteps in grad school and beyond.

I also want to thank Dr. Bevly for offering me this opportunity. As a senior in college I had no clue what I wanted to do with my life. By allowing me the opportunity to work in his lab, I have discovered what I love to do and have found a whole world of opportunities that I never knew existed. I also want to thank everyone in the GAVLAB who has helped me on my journey, especially Ryan and Joe for always being willing to sacrifice their time to go collect data with me again..and again...and again in the midsummer heat.

And finally I want to thank all my friends at Church of the Highlands. Because of them, Auburn became more than just my college, it became my home. Although it pains me to say goodbye to the friends I have made over the past couple years, I know that we will see each other again in the future.

Table of Contents

List of Figures

Chapter 1

Introduction

Since the advent of GPS, research in the area of improving navigation continues to increase as GPS sees more usage in all aspects of daily life. Originally, GPS allowed a user to locate their position anywhere on the earth to within a few meters. Now, there are methods available to not only locate a user's position to sub-meter level, but to precisely measure velocity and attitude as well. Research on improving GPS navigation is fueled by the needs of both military and civilian applications that require extremely precise navigation solutions, whether it be guided munitions or autonomous vehicles. One of the most common navigation tools is the GPS/INS system. An INS, or inertial navigation system, is the result of propagating the measurements from an inertial measurement unit (IMU) to obtain position, velocity, and attitude. IMUs measure acceleration and angular rates, with some also measuring magnetic fields, barometric pressure, and more. The advantages of using GPS/INS are its accuracy and fast update rate, however it still suffers from several flaws that can limit reliability for critical applications. GPS requires constant line-of-sight to the GPS satellites, and the signal can be blocked or corrupted by structures or the natural landscape around a vehicle. On the other hand, the IMUs used in GPS/INS systems commonly suffer from errors such as noise and bias drift, and if not corrected by accurate GPS measurements can lead to degraded navigation solutions over time.

1.1 Prior Work and Contributions

Much work has been devoted to improving the position, velocity, and attitude (PVA) estimates of the GPS/INS navigation filter. When designing a navigation filter, one of the first choices to be made is the quality of the IMU. In [20], the author explains the differences

between IMU qualities and develops a tool to help aid a designer in making the right choice for the application. There are also ways to aid a navigation solution produced by the GPS/INS filter. A common tool used for navigation aiding is the magnetometer. Magnetometers are useful in heading stabilization or attitude determination [9]. In [42], a magnetometer was used to detect magnetic anomalies, which can be used as a marker to correct any drift or bias in a navigation solution. Magnetometers have also been used in a spacecraft for attitude determination [5]. Finally, in [36], a magnetometer based attitude determination algorithm was used to produce an attitude measurement that could be used in the measurement update of a closely-coupled filter that improves the observability of the states in a GPS/INS Kalman Filter.

In other applications, radars have been used for GPS/INS aiding. Although radars have been around longer than GPS, its use as a civilian vehicle navigation aid has not been studied as extensively as GPS due to the fact that radar only has limited range and is not available everywhere on earth at any given instance. However, radars can have many practical applications, especially in areas where GPS may not be available, such as an urban canyon within a city. In [38], a radar from a navy ship was used to aid GPS measurements in missile system navigation, because the object to be guided was moving too fast for GPS to accurately provide a navigation solution. For a more consumer-based application, radar was used as an aid to dynamic real-time kinematic (DRTK) navigation for relative positioning between two vehicles [43],.

In light of all the research that has been done to improve the navigation solutions produced by GPS/INS systems, there are still areas that have yet to be explored. The major contribution of this thesis is to use previous research and create a new navigation filter that seeks to take IMU measurements and fuse them with radar and magnetometer-based attitude measurements in an Extended Kalman Filter. This new filter is called the radar-aided INS (RAINS) navigation filter. This filter eliminates some problems associated with GPS, most prominently loss of signal, by replacing GPS with radar measurements to

a known location. The inclusion of a magnetometer to obtain attitude measurements allows for the use of the radar. This is due to the fact that without attitude measurements, the filter uncertainty would grow indefinitely and no navigation solution would be possible, as will be shown in this thesis. With this in mind, the next sections give a brief background on magnetic sensing technology, inertial measurement units, and radar measurements along with some of the difficulties involved in implementing these sensors effectively.

1.2 Magnetic Measurements

1.2.1 Background

Using the earth's magnetic field for navigation is not a recent discovery. The compass has been used to give explorers and navigators a heading reference for almost 2000 years [29]. Though the technology has advanced far beyond a simple magnetized needle, the principle remains the same. Today, magnetometers are the state-of-the-art tool for utilizing earth's magnetic field as a navigation aid. Magnetometers are sensors that operate by measuring magnetic fields around them, and can either be scalar or vector magnetometers. Scalar magmetometers measure only the strength of the magnetic field around them, while vector magnetometers measure both magnitude and direction. Magnetometers have seen much use in navigation aiding, including use in spacecraft [5, 47], air vehicles [9, 16], pedestrian navigation [22, 30], and mining and surveying [19].

In many applications, magnetometers are measuring the earth's magnetic field. Earth's magnetic field operates similar to a magnet, with the field always pointing from the south to the north pole (see Figure 1.1). The components of the magnetic field that are parallel to the surface of the earth can be used to find a vehicle's heading. There are several models available for representing the earth's magnetic field, but for this thesis the International Geomagnetic Reference Field (IGRF) is used [24].

Magnetometers, especially vector magnetometers, have proved their usefulness in many navigation situations. When the magnetic field strength and direction is measured in a

3
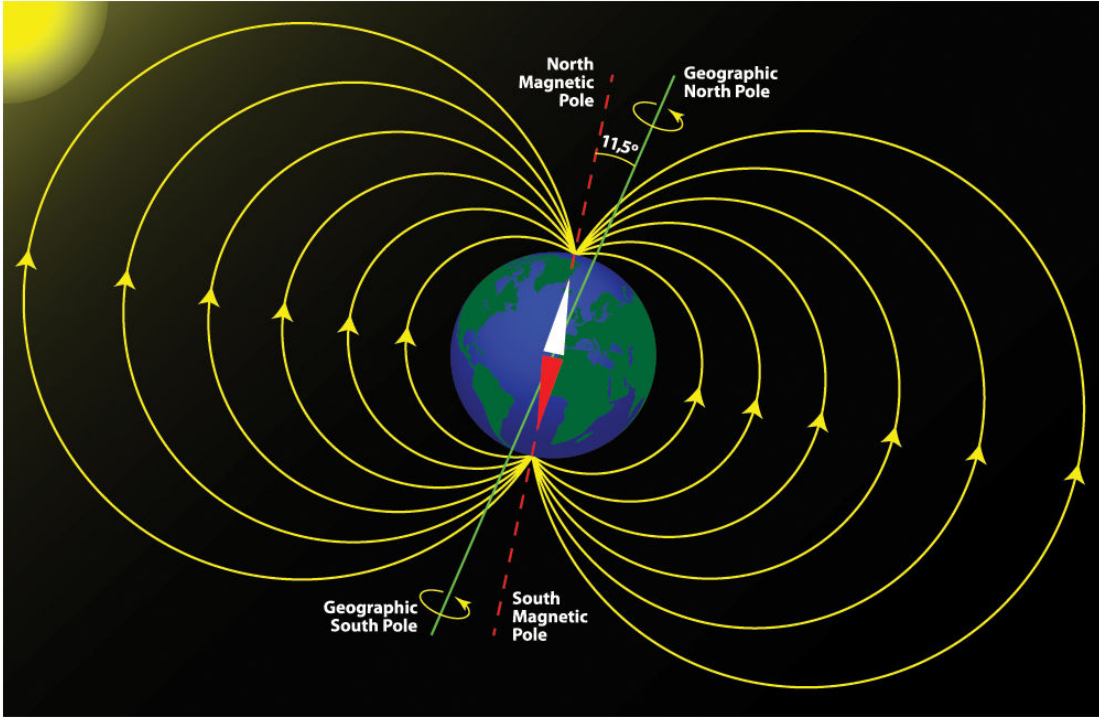
Figure 1.1: Illustration of the Earth's magnetic field [12]

vehicle with no pitch or roll, the heading (ψ) can be easily calculated using the simple equation

$$\psi = atan2(b_y, b_x) \tag{1.1}$$

where using the 4-quadrant inverse tangent will yield heading for a full 360 degrees, and b_x and b_y are the magnetometer measurements in the x and y direction, respectively. For this reason, vector magnetometers find the most use in navigation. In addition to heading calculation, magnetometers can also be used for map-matching navigation [42] and 6 degree of freedom (DOF) attitude determination [17,31]. In this thesis, the magnetometer is used to determine 6-DOF attitude, which will be further discussed later.

1.2.2 Magnetometer Error Sources

In most applications, magnetometers will be measuring disturbances as well as the earth's magnetic field. If there is a material producing its own magnetic field nearby, such as a magnet or a motor, then the magnetometer measurement will become biased relative to the earth's magnetic field. If there is a ferrous material nearby, then the magnetic field will become distorted. These bias and scaling errors are known as a hard iron bias and soft iron bias, respectively. Figure 1.2 shows what the error-free magnetometer measurements should look like, and how hard and soft iron bias change those measurements.

(a) Perfect Magnetometer Measurements

(b) Magnetometer Measurements with Hard Iron Bias

(c) Magnetometer with Soft Iron Bias

Figure 1.2: Effects of Hard and Soft Iron Bias on Magnetometer Measurements

As shown in the Figure 1.2a, perfect measurements will result in a circle centered about (0,0). If there is hard iron bias, as in Figure 1.2b, the measurements will be off-center. In the presence of soft iron bias, shown in Figure 1.2c, the measurements are centered,

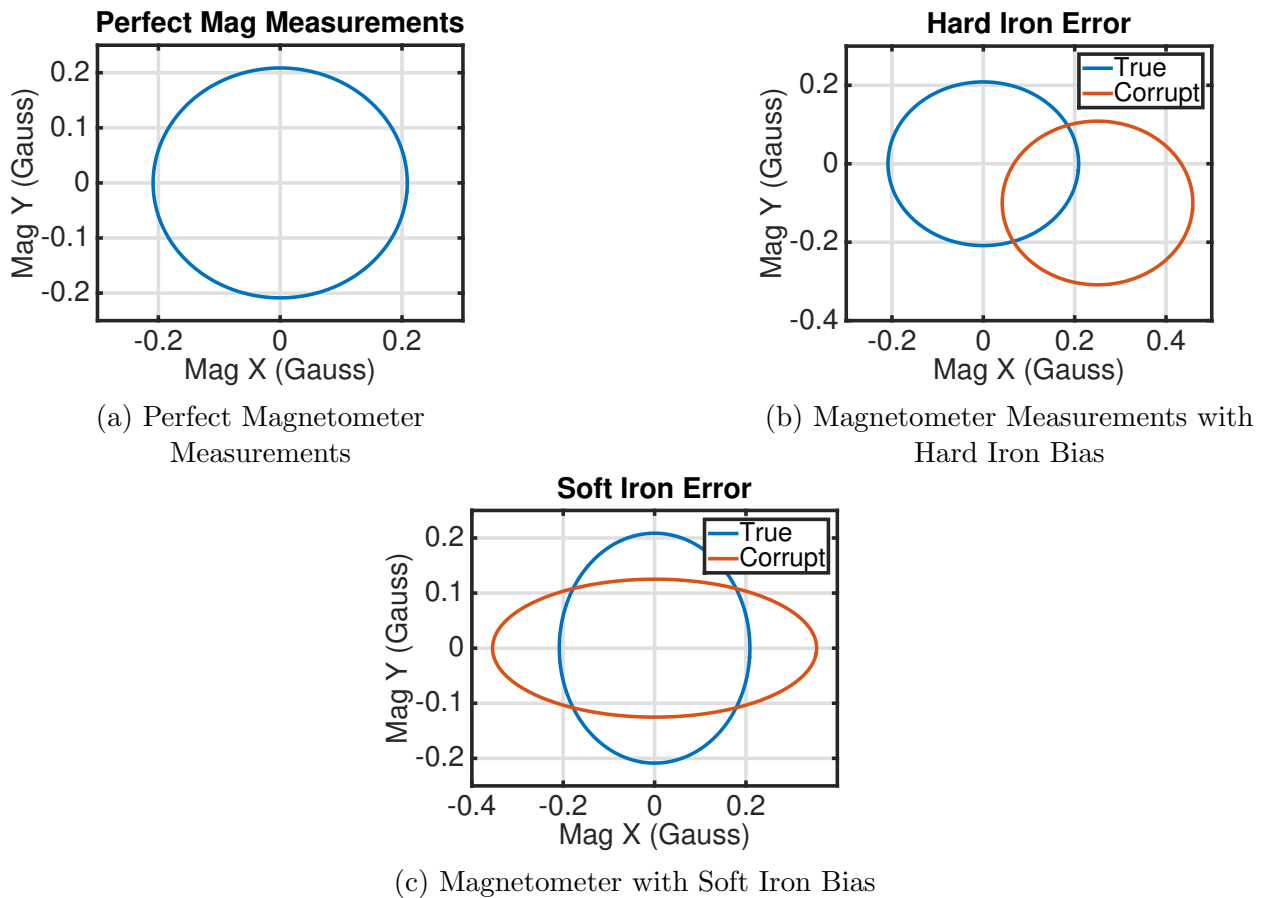but the magnitudes are skewed and the circle becomes an ellipse. In addition to these errors, magnetometers will also be subject to common IMU errors such as wide-band noise. Errors can also arise if the magnetometer is not aligned with the vehicle. For example, if the magnetometer were rolled several degrees with respect to the vehicle, the y-axis of the magnetometer would not be measuring the true y-component of earth's magnetic field. Instead, it would be measuring a mix of the y- and z-components of the earth's magnetic field. This difference can result in corrupt heading estimates. To reduce or eliminate the errors caused by hard and soft biases and misalignment, the magnetometer must be calibrated, which will be covered in detail later in Chapter 2.

1.3 Inertial Measurement Units

Inertial Measurement Units (IMU) are sensors that contain at least some combination of accelerometers and gyroscopes. As magnetometers begin to show increasing promise as a navigation aid, IMUs have begun to incorporate magnetometers into their sensor suite as well. The work done in this thesis depends on magnetic measurements, so an IMU with a magnetometer included was chosen to gather experimental data. As stated earlier, there are various levels of quality of IMUs. The noise characteristics of the IMU will depend on the quality. Marine-grade IMUs offer the longest term stability with the the least amount of bias and drift, but can cost up to one million dollars. Consumer grade IMUs are available for the lowest cost, but cannot give an accurate navigation solution on their own for more than a few seconds. Table 1.1 lists the different levels of IMUs and the bias associated with each [21].

Accelerometers operate on the principle of measuring the displacement of a proof mass. When the IMU is subject to an acceleration, the proof mass will shift relative to the sensitive axis and compress a spring. By measuring the displacement of this proof mass, the acceleration can be calculated. Gyroscopes measure the angular rates of the IMU about a

Table 1.1: Common Bias Values for IMU Grades [21]

IMU Grade	Accelerometer Bias (m/s^2)	Gyroscope Bias (rad/s)
Marine	10^-4	$5x10^-9$
Aviation	$3x10^-4 - 10^-3$	$5x10^-8$
Intermediate	$10^-3 - 10^-2$	$5x10^-7$
Tactical	$0.01 - 0.1$	$5x10^-6 - 5x10^-4$
Automotive	> 0.03	$5x10^-4$

sensitive axis. Two common types of gyroscopes are optical and vibratory, and measure the angular rates using principles such as the Sagnac Effect and Coriolis acceleration [21].

The technique of integrating and propagating IMU measurements to obtain a position, velocity, and attitude solution is known as an Inertial Navigation System (INS), which is a type of dead reckoning. To demonstrate the effects bias has on dead reckoning, a simple trajectory of a vehicle travelling in a circle at a constant tangential velocity for thrity seconds was created in simulation. From this trajectory, IMU measurements were generated to simulate various IMU grades represented in Table 1.1. These IMU measurements were then propagated in an inertial navigation system to obtain the measurement for position after a single run. The position error is shown in Figure 1.3. As can be seen, the marine-grade IMU creates the best estimate, with sub-meter level accuracy. However, the tactical and automotive grade position estimates begin to drift rapidly. The results of this test show where the motivation arises to aid IMUs. Aiding allows the use of cheaper IMUs while still getting an accurate navigation solution that will not drift over time.

1.4   Radar Background

This section provides a brief history of radar. If more information on the subject is desired, [50] provides a more in-depth look at its history and development. The word "radar" is an acronym that stands for "RAdio Detection And Ranging." Radar was first demonstrated as early as 1886 by German physicist Heinrich Hertz, who showed that radio waves could be reflected from solid objects (Figure 1.4) [23]. This principle was not thoroughly studied
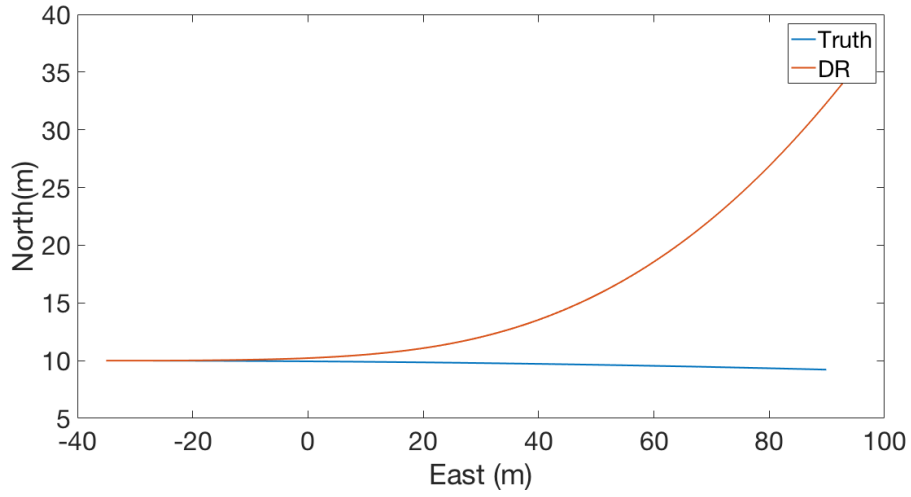
(a) Dead-Reckoned Position with an Automotive-Grade IMU
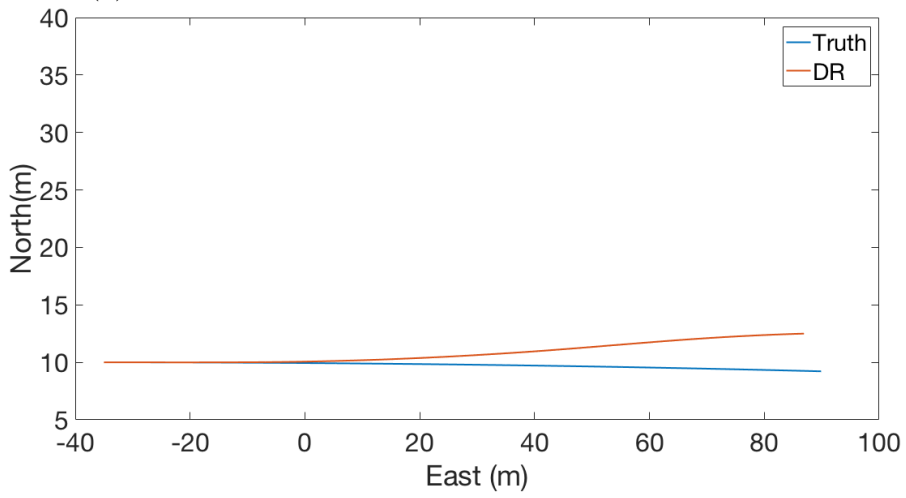
(b) Dead-Reckoned Position with a Tactical-Grade IMU
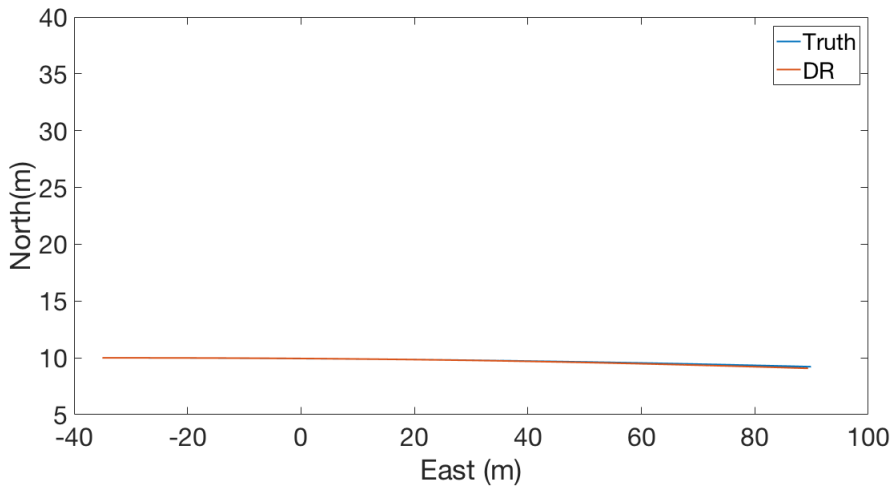
(c) Dead-Reckoned Position with a Marine-Grade IMU

Figure 1.3: Dead-Reckoned Position for Various Grades of IMU

in earnest until the onset of World War 2, where radar played a critical role in Britain by providing early warning of German aircraft [8]. With the full potential of radar demonstrated, many nations began pouring resources into further developing their radar capabilities [8]. Today, radars are used in air traffic control, weather prediction and modeling, munitions guidance, marine navigation, and autonomous vehicles [1, 13] . Radar works by emitting radio waves and measuring the signal that gets reflected back off an object. From the reflected signal, a radar can calculate the location and speed of that object. Of course, this is a very simplistic way of viewing radar. For a more comprehensive review of the design and workings of radar, see [46].

Figure 1.4: Basic Diagram of Radar Operation [7]

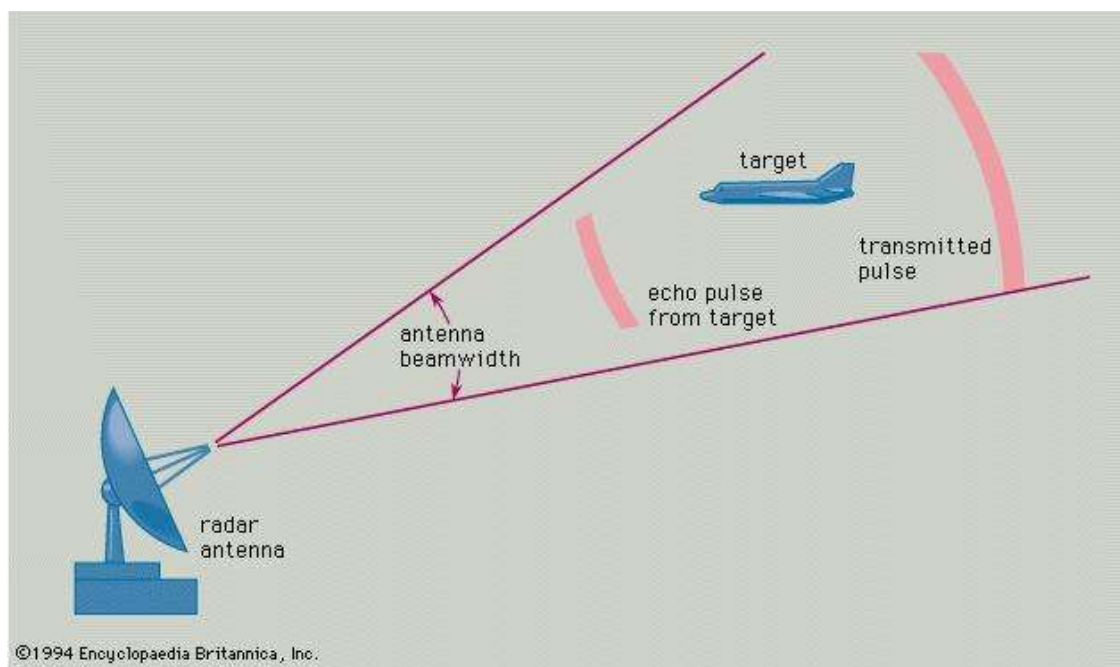One of the major problems that plague radars is target acquisition. A radar will create measurements for every signal that gets reflected back to it, so there will be many non-valid "targets" that obscure the true measurements, which is known as "clutter." To eliminate clutter, an algorithm is needed that either filters the measurements to eliminate erroneous

signals, or can statistically predict what the radar should be measuring. This process of target acquisition will be further discussed in Chapter 5.

1.5 Conclusions

In this chapter, the motivation for this thesis was presented and several methods for aiding the GPS/INS system were reviewed. Although GPS/INS is a well-know and dependable tool for navigation, it does have drawbacks with IMU errors when loss of GPS signals occurs. A brief overview of magnetic sensing technology and the errors associated with it was given. Inertial Measurement Units were introduced, and how quality can affect the long-term performance an IMU. A short history of radar technology was given along with a simple explanation on how radars operate and the issue of radar target acquisition. The goal of this thesis seeks to utilize these methods in a new filter that uses radar and magnetometer-based attitude measurements. Chapter 2 will cover how the magnetometer is calibrated for the experiments performed, with calibration results shown in simulation and experimentally. The use of magnetometers for attitude determination will be shown in Chapter 3. INS navigation and INS aiding in Kalman Filters will be covered in Chapter 4. In Chapter 5, radar target determination will be discussed, and the new filter proposed by this thesis will be tested in simulation and experimentally. The results will demonstrate how combining radar and attitude measurements with an inertial navigation system to create a new navigation filter enables estimation of a vehicle's position, velocity, and attitude without GPS measurements. Finally, conclusions and future work will be provided in Chapter 6.

Chapter 2

Magnetometer Calibraton

2.1 Introduction and Prior Work

To use a magnetometer in order to accurately calculate attitude, magnetometer errors must be accounted for through magnetometer calibration. Magnetometer calibration has been an area of extensive research for many years. All calibrations fall into either 2-dimensional or 3-dimensional categories. With 3-dimensional calibration, the magnetometer can be used to calculate the full attitude of a vehicle, however in many ground vehicle situations the third axis calibration is poor due to observability issues. If only heading is desired instead of full attitude, then two-dimensional calibrations can be used. Caruso's method provides a quick and easy way to accurately calibrate the magnetometer in two axes [10], and can even handle small amounts of pitch and roll. Kwanmuang et. al. developed a calibration procedure for pedestrian dead reckoning (PDR) heading calculation [30]. Two-dimensional calibration has advantages with lower computational requirements and accuracy within just a couple degrees for systems with low amounts of pitch and roll. However, for this thesis, it was desired to have a calibration routine that would calibrate all three axes so the magnetometer measurements could easily be applied to six degree-of-freedom vehicles such as aircraft. Koo et. al. use a particle filter for 3-axis calibration, but requires the use of multiple IMUs to level the magnetic measurements [28], which increases the cost of the navigation system. Alonso and Shuster then present their calibration algorithm, called TWOSTEP [2], which is a 3-axis calibration that does not require other sensors to operate. The TWOSTEP calibration improves on older calibration routines, and has been demonstrated in various situations to hold up well against other calibration algorithms [3,4]. However, the TWOSTEP calibration routine was designed for spacecraft and does not hold well for in-atmosphere

vehicles. In [18], Gebre-Egziabher presents a method for 3-axis magnetometer calibration that can be performed with no a priori knowledge of attitude. Because of this algorithm's efficiency and accuracy of results, and based on the previous work done in [36], this method was chosen as the calibration routine of choice for this thesis.

2.2 Gebre-Egziabher Calibration

The Gebre-Egziabher calibration routine seeks to fit the data from a magnetometer to an ellipsoid of best fit centered about the origin by using a model of the earth's magnetic field. The calibration process first involves a batch least-squares estimator to generate initial estimates of the hard and soft iron bias. Next, an iterative least squares process is performed to refine the bias estimates until convergence is achieved. This calibration routine can accurately estimate the hard and soft iron bias, represented by (b_x, b_y, b_z) and $(\gamma_x, \gamma_y, \gamma_z)$, respectively. The routine does not estimate misalignment errors but instead lumps misalignment into the soft iron bias estimates. To calibrate the magnetometer, the problem must be formulated as the least-squares equation of the form

$$\vec{x} = (H^T H)^{-1} H^T \vec{y} \tag{2.1}$$

where $\vec{x}$ is the vector of parameters that need to be estimated as defined in Equation (2.5). To compute the error parameter estimates, an accurate error model is needed, shown by

$$h^2 = \left(\frac{\tilde{h}_x^b - b_x}{\gamma_x} \right)^2 + \left(\frac{\tilde{h}_y^b - b_y}{\gamma_y} \right)^2 + \left(\frac{\tilde{h}_z^b - b_z}{\gamma_z} \right)^2 \tag{2.2}$$

where h is the magnitude of the earth's magnetic field model, and $\tilde{h}^b$ represents the magnetometer measurements in each axis. By expanding Equation (2.2), Equation (2.3) is formed.

$$h^2 = \frac{(\tilde{h}_x^b)^2 - 2(\tilde{h}_x^b)(b_x) + (b_x)^2}{\gamma_x^2} + \frac{(\tilde{h}_y^b)^2 - 2(\tilde{h}_y^b)(b_y) + (b_y)^2}{\gamma_y^2} + \frac{(\tilde{h}_z^b)^2 - 2(\tilde{h}_z^b)(b_z) + (b_z)^2}{\gamma_z^2} \tag{2.3}$$

Given that there will be k magnetometer measurements, k instances of Equation (2.3) can be created. After rearranging the k expressions of Equation (2.3), a matrix equation of the form

$$\vec{y} = H\vec{x} + \vec{\nu} \tag{2.4}$$

can be written as

$$
-\begin{bmatrix}
(\tilde{h}_x^b(t_1))^2 \\
(\tilde{h}_x^b(t_2))^2 \\
(\tilde{h}_x^b(t_3))^2 \\
\vdots \\
(\tilde{h}_x^b(t_{k-1}))^2 \\
(\tilde{h}_x^b(t_k))^2
\end{bmatrix}
=
\begin{bmatrix} H_{11} H_{12} \end{bmatrix}
\begin{bmatrix}
b_x \\
\mu_2(b_y) \\
\mu_3(b_z) \\
\mu_2 \\
\mu_3 \\
\mu_4
\end{bmatrix}
+ \vec{\nu} \tag{2.5}
$$

where $\vec{\nu}$ represents the measurement noise, and H is composed of two $(k x 3)$ submatrices defined as

$$
H_{11} =
\begin{bmatrix}
-2\tilde{h}_x^b(t_1) & -2\tilde{h}_y^b(t_1) & -2\tilde{h}_z^b(t_1) \\
-2\tilde{h}_x^b(t_2) & -2\tilde{h}_y^b(t_2) & -2\tilde{h}_z^b(t_2) \\
-2\tilde{h}_x^b(t_3) & -2\tilde{h}_y^b(t_3) & -2\tilde{h}_z^b(t_3) \\
\vdots & \vdots & \vdots \\
-2\tilde{h}_x^b(t_{k-1}) & -2\tilde{h}_y^b(t_{k-1}) & -2\tilde{h}_z^b(t_{k-1}) \\
-2\tilde{h}_x^b(t_k) & -2\tilde{h}_y^b(t_k) & -2\tilde{h}_z^b(t_k)
\end{bmatrix}
\tag{2.6}
$$

$$H_{12} = \begin{bmatrix} (\tilde{h}_y^b(t_1))^2 & (\tilde{h}_z^b(t_1))^2 & 1 \\ (\tilde{h}_y^b(t_2))^2 & (\tilde{h}_z^b(t_2))^2 & 1 \\ (\tilde{h}_y^b(t_3))^2 & (\tilde{h}_z^b(t_3))^2 & 1 \\ \vdots & \vdots & \vdots \\ (\tilde{h}_y^b(t_{k-1}))^2 & (\tilde{h}_z^b(t_{k-1}))^2 & 1 \\ (\tilde{h}_y^b(t_k))^2 & (\tilde{h}_z^b(t_k))^2 & 1 \end{bmatrix} \tag{2.7}$$

The μ terms in the state vector shown in Equation(2.5) are defined as

$$\mu_1 = h^2 \gamma_x^2 \tag{2.8}$$

$$\mu_2 = \frac{\gamma_x^2}{\gamma_y^2} \tag{2.9}$$

$$\mu_3 = \frac{\gamma_x^2}{\gamma_z^2} \tag{2.10}$$

$$\mu_4 = (b_x)^2 + \mu_2(b_y)^2 + \mu_3(b_z)^2 - \mu_1 \tag{2.11}$$

Since Equation (2.5) is in a common state-space format, the state vector can be solved for using Equation (2.1). Using the solution for the state vector, the hard and soft iron bias can then be calculated using Equations (2.8 -2.11).

As stated earlier, this batch least-squares estimate is only the initial estimate of the error terms. However, in [18], Gebre-Egziabher shows that often times, the initial estimate is good enough for accurate calibration. The accuracy of the initial estimate was further validated in [36]. For that reason, only the initial estimates were used in this thesis. Also, the state vector has been slightly modified from what was presented in [18]. The fourth term

14

in $\vec{x}$ has been changed from a μ_1 to a μ_2 to better represent the model. This change can be determined through inspection of Equation (2.3), and again was further validated in [36].

The calibration routine was evaluated with both simulated and experimental data. First, the simulated case will be presented, then the experimental results will be discussed. Both cases will compare the post-calibration magnetic heading to a "truth" reference to validate that the magnetometer has been accurately calibrated.

2.3   Calibration with Simulated Data

To simulate magnetometer measurements in MATLAB, the IGRF model of the earth's magnetic field was rotated 360 degrees about the vertical axis. Since the calibration from [18] is seeking to fit an ellipsoid of best-fit to a magnetic model, it is essential that at least 360 degrees of rotation in one plane is gathered for the batch least-squares estimation, otherwise the estimates will diverge. The authors also state that the estimates are improved by the measurements being rotated out of the 2-dimensional plane, which is often the case seen in real world use. To test the calibration in simulation, magnetometer measurements were generated by using the IGRF magnetic model, and rotating those about the magnetometer's z-axis. To create "corrupted" magnetometer measurements, Equation (2.12) was used.

$$\tilde{h^b} = (h^b + b)\gamma \tag{2.12}$$

In this equation, h^b represents the true magnetic measurement from the IGRF data at a location in Auburn, AL, b is the hard iron bias, γ is the soft iron bias, and $\tilde{h^b}$ is the measured magnetic field from the magnetometer. On top of the hard and soft iron bias, the magnetic measurements were also rolled by 9 degrees and pitched by 5 degrees and had random noise with a standard deviation of .005 milliGauss added. These corrupted measurements were then calibrated using the previously described calibration routine. Figure 2.1 shows the perfect magnetometer measurements without any biases, roll, pitch, or noise, and Figure

2.2 shows the magnetometer measurements corrupted by hard and soft iron bias, pitch, roll, and white, Gaussian noise. The calibrated magnetometer can be seen in Figure 2.3, where the measurements have been re-centered on the origin and rescaled. Even with the added pitch and roll, there is still not enough variation to accurately calibrate the z-axis , so the calibration results in z-axis measurements close to 0. This discrepency occurs because the data collected does not provide enough variation in the z-axis measurements, so the calibration seeks to shift the locus of data to the origin in the z-axis as well as the x- and y-axes. To evaluate the calibration, a comparison of the heading calculations are shown in Figure 2.4. As can be seen, the calibrated magnetometer heading matches very closely with the true heading with only noise present in the calibrated measurements. This shows that the calibration routine is correctly estimating the hard and soft bias errors.
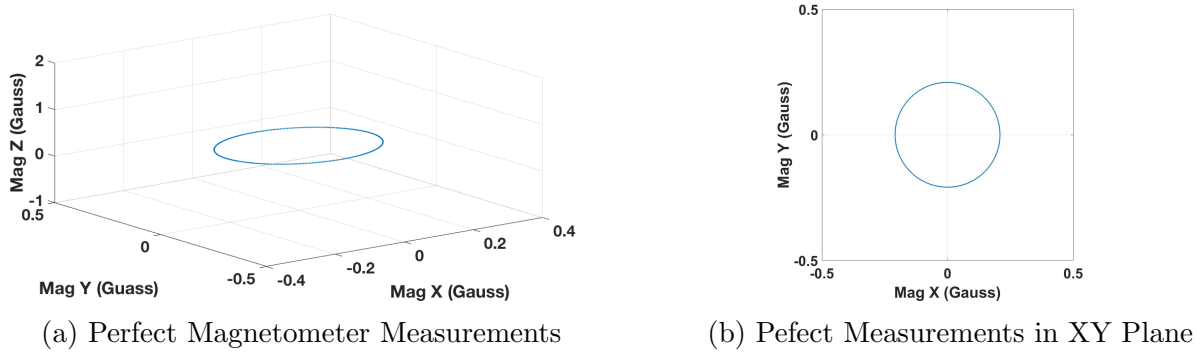

(a) Perfect Magnetometer Measurements

(b) Pefect Measurements in XY Plane

Figure 2.1: Perfect Simulated Magnetometer Measurements

(a) Corrupted Magnetometer Measurements

(b) Corrupted Magnetometer Measurements in XY Plane
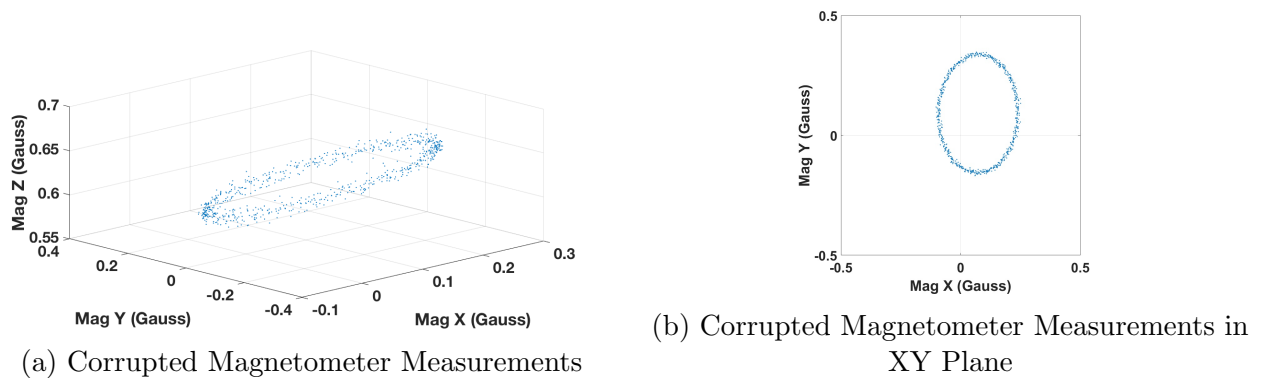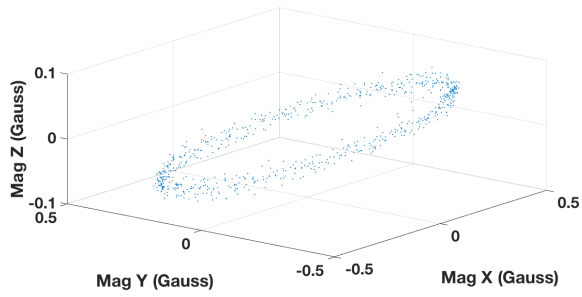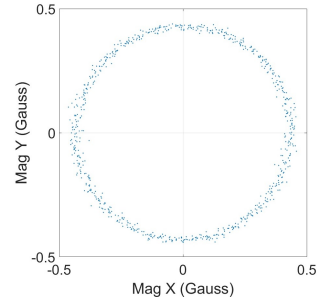
Figure 2.2: Corrupted Simulated Magnetometer Measurements

(a) Calibrated Magnetometer Measurements

(b) Calibrated Magnetometer Measurements in XY Plane

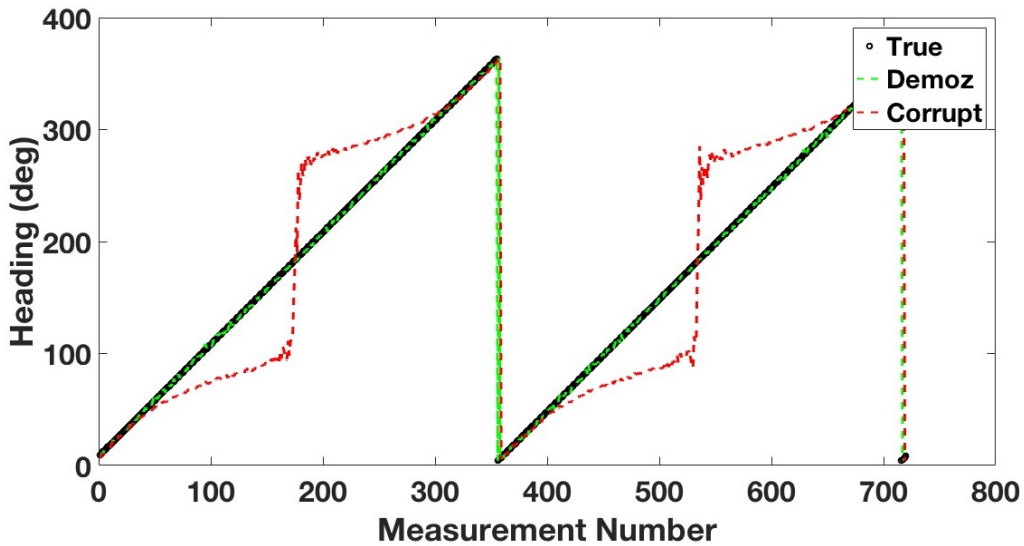Figure 2.3: Calibrated Simulated Magnetometer Measurements

Figure 2.4: Simulated Magnetometer Heading

2.3.1 Experimental Results

Once the calibration routine was validated using simulated measurements, the calibration was then tested using experimental data. To test the routine, an Xsens MTi IMU (Figure 2.5) was mounted in an Infiniti G35 (Figure 2.6). The vehicle also has a three antenna Septentrio GPS receiver that was used as the "truth" for heading calculation. The vehicle was driven to approximately the same location that was used for the IGRF data in the simulation and driven in several circles to collect data in at least 360 degrees of rotation.

The data was then calibrated in post-process, and the magnetometer measurements were used to calculate heading.


Figure 2.5: Xsens MTi

Figure 2.6: Infiniti G35

The raw magnetometer measurements are shown in Figure 2.7. It can be seen in the plots that the magnetometer suffers from hard iron bias, especially in the x-axis, and a small amount of soft iron bias that is causing the measurements to be ellipsoidal in shape. After calibrating the magnetometer, the measurements have been re-centered and corrected for any scale-factor errors, as shown in Figure 2.8. However, the calibration routine still results
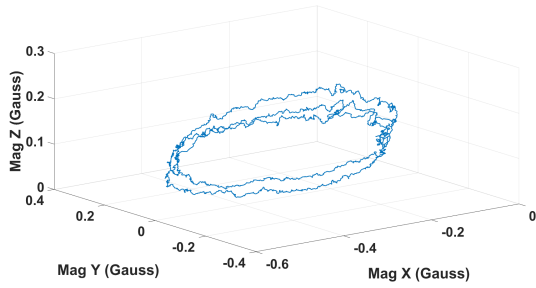
(a) Uncalibrated Magnetometer Measurements
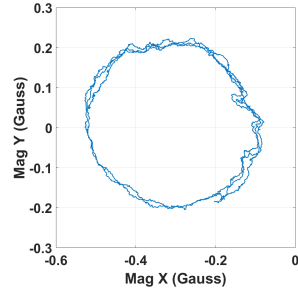
(b) Uncalibrated Magnetometer Measurements in XY Plane

Figure 2.7: Uncalibrated Experimental Magnetometer Measurements
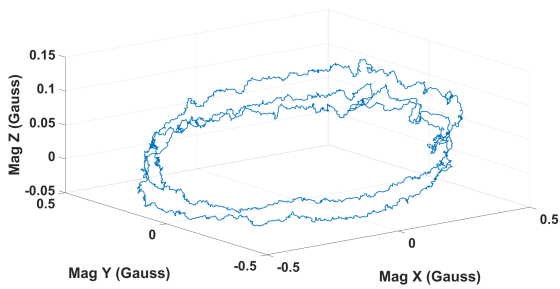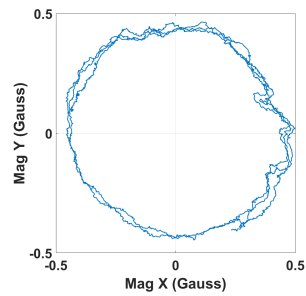

(a) Calibrated Magnetometer Measurements

(b) Calibrated Magnetometer Measurements in XY Plane

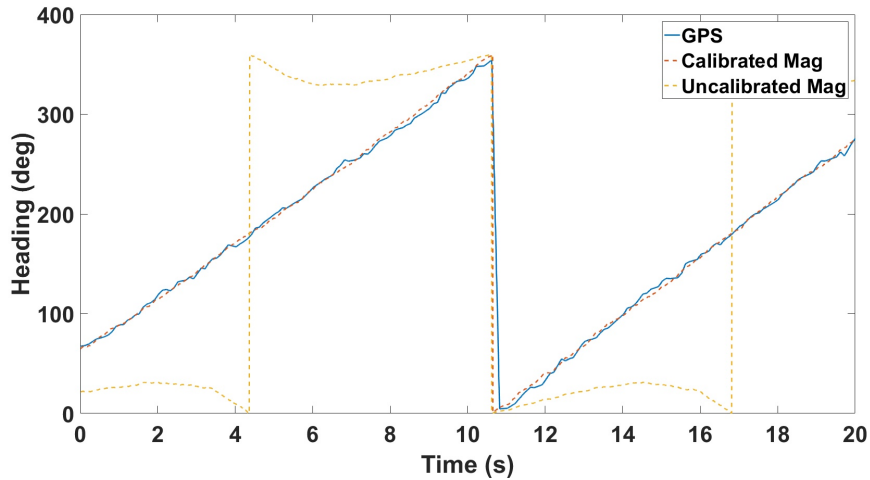Figure 2.8: Uncalibrated Experimental Magnetometer Measurements

Figure 2.9: Vehicle Heading for Raw and Calibrated Mag and Septentrio Measurements

in z-axis measurements at zero because there was not enough pitch and roll in the vehicle to accurately calibrate the z-axis.

To check that heading accuracy has been maintained throughout the calibration process, the calibrated magnetometer heading was compared to the measured Septentrio heading. Figure 2.9 shows a plot of all three heading measurements. The raw measurements are strongly corrupted by the hard and soft iron biases, and are unable to estimate heading. The calibrated magnetometer measurements estimate a much more accurate heading, and are close to the true value. The error between the Septentrio heading and the calibrated magnetometer calculated heading is shown in Figure 2.10. After calibration, the heading error is never larger than four degrees. The resulting mean error for the calibrated heading is -.0262 degrees with a standard deviation of 1.4921 degrees. The experimental results show that the selected calibration routine is valid, and will yield accurate results when calculating heading. It will be important to know that the magnetometer is being correctly calibrated when trying to determine a vehicle's attitude, which will be discussed later in this thesis.
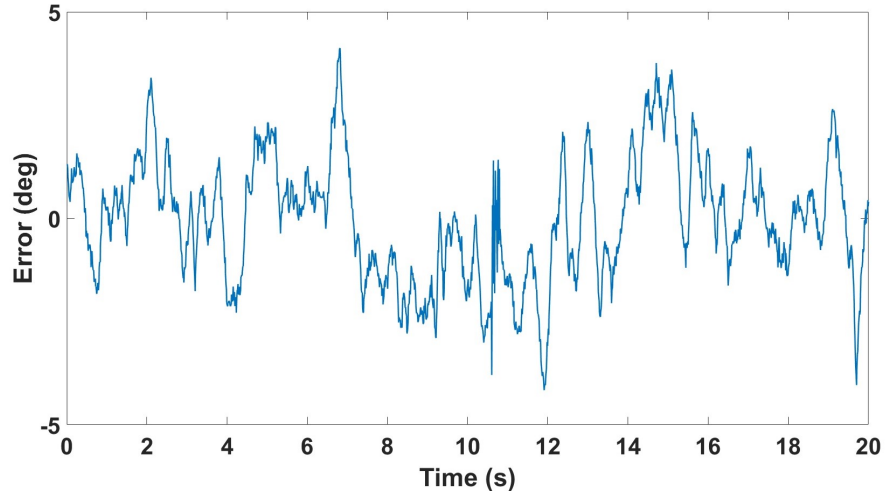
Figure 2.10: Vehicle Heading Error for Calibrated Magnetometer Measurements

2.4   Conclusion

Extensive research has been devoted to develop faster, more robust, and more accurate magnetometer calibration under many conditions. For this thesis, one calibration algorithm was chosen that met the needs for accuracy, efficiency, and robustness and could be applied to an in-atmosphere 6 degree-of-freedom vehicle. This calibration was tested in simulation, and then verified by collecting experimental data using an Xsens MTi IMU in an Infiniti G35. Both the simulated and experimental results show that this algorithm can calibrate a magnetometer to obtain accurate heading estimates.

Chapter 3

Magnetometer-Based Attitude Determination

3.1 Background and Previous Work

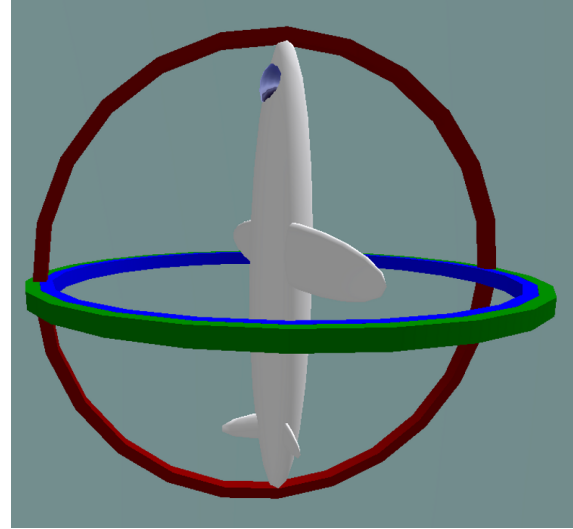While magnetometers can be used soley for vehicle heading calculation, they are also useful in six degree-of-freedom (DOF) attitude determination. To correctly navigate and control a vehicle, whether it is an air vehicle [17], a spacecraft [45], or a ground vehicle, it is important to know how the vehicle is oriented in the navigation frame. Thus, there is a need to determine the vehicle's attitude. The process of combining different sensors into an algorithm to determine attitude is called an Attitude Heading and Reference System, or AHRS. In 1965, Grace Wahba proposed that the attitude of one coordinate frame relative to another could be found using a set of vector measurements [49]. Each coordinate frame must contain a set of at least two vectors, and each vector in that set must have a corresponding vector in the opposing coordinate frame that points to the same point as itself. Under these conditions, the problem is solving a rotation between the vector sets that will be the same as the rotation between coordinate frames.

Wahba developed a solution when first proposing the problem by minimizing a least-squares loss function with n vectors, where $n \geq 2$. Since then, much research has been devoted to improving the accuracy and efficiency of the solution and on how to incorporate different sensors. The matrices representing the rotation between the coordinate frames is usually represented in either Euler angles or quaternions, with quaternions being a more common choice due to the fact that there are no angular singularities that can occur with Euler angles [15]. For example, if an aircraft is flying straight up relative to the navigation frame, then roll is not observable, and yaw and pitch are indistinguishable from each other. This is a common problem known as gimbal-lock, shown in Figure 3.1.
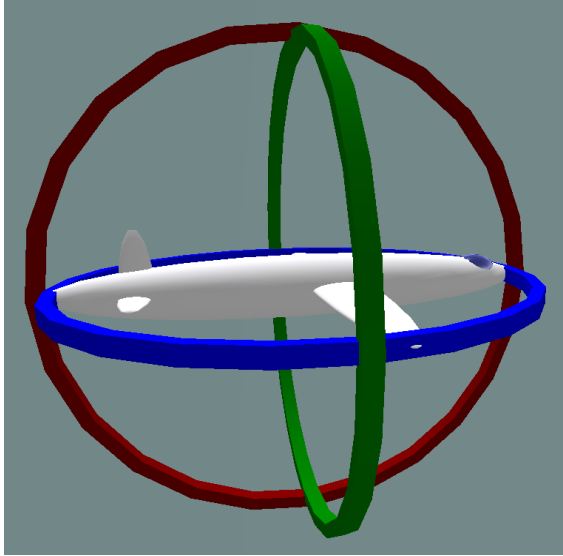
(a) Normal Operating Conditions [34]   (b) Gimbal Lock Conditions [35]

Figure 3.1: Example of a Gyroscope Under Normal and Gimbal Lock Conditions

Most AHRS algorithms can be broadly placed in one of two categories, optimal and deterministic. Deterministic solutions use a minimal data set to derive the attitude with nonlinear equations, while optimal algorithms use two or more data sets to compute the attitude by minimizing an appropriate cost function solution [48]. Shortly after Wahba's problem was proposed, Davenport produced his own deterministic least-squres solution for attitude determination using Euler angles, but the solution still had one singularity [14]. Another deterministic solution, TRIAD, computed attitude by restricting the data to two unit-vector pairs [44]. Later, optimal solutions were developed in the form of QUaternion ESTimator (QUEST) [37] and the EStimators of the Optimal Quaternion (ESOQ) [44]. These algorithms avoid singularities because they estimate quaternions instead of Euler angles, and they are both much faster than Davenport's solution. However, neither of these solutions are as robust as Davenport's solution. Since determinstic solutions involve solving cumbersome, nonlinear equations, most research has been devoted to optimal solutions. For this reason, the optimal attitude determination algorithm presented in [31] was used for this thesis. This algorithm estimates the rotation quaternion through an iterative Gauss-Newton method. It was chosen because it is more robust then the QUEST and ESOQ algorithms,

but more computationally efficient than Davenport's solution. The algorithm is described in more detail in the following section.

3.2   Attitude Determination

As stated earlier, in order to determine the rotation of one coordinate frame to another, there must be a set of at least two vectors in each coordinate frame that point to corresponding points. For example, in a body frame and a navigation frame, the accelerometer would be measuring gravity effects, corresponding with earth's gravity model. Let the two vectors in the navigation frame be represented by $\underline{y_e^1}$ and $\underline{y_e^2}$, with corresponding vectors in the body frame represented by $\underline{y_b^1}$ and $\underline{y_b^2}$. There exists between these vector sets a rotation matrix such that

$$\underline{y_e^1} = R_b^e \underline{y_b^1} \tag{3.1}$$

$$\underline{y_e^2} = R_b^e \underline{y_b^2} \tag{3.2}$$

where R_b^e is the rotation matrix between the coordinate frames. The vectors in the navigation frame can come from any vector measurement sensors, such as star sensors, horizon sensors, accelerometers, or magnetometers, to name a few. These measurements must then correspond to the model used in the navigation frame. For this thesis, an accelerometer and magnetometer were used for the vector measurements $\underline{y_b^1}$ and $\underline{y_b^2}$, while the earth's magnetic field model and gravity model were used for $\underline{y_e^1}$ and $\underline{y_e^2}$. In the first vector set, the magnetometer measurements will correspond to the magnetic field model, and for the second vector set, the accelerometer measurements will correspond to the gravity model. The algorithm seeks to minimize the error function H defined as follows

$$H = \epsilon^T \epsilon = (\underline{y_e} - M\underline{y_b})^T (\underline{y_e} - M\underline{y_b}) \tag{3.3}$$

With magnetic measurements indicated by $\underline{m}$, and accelerometer/gravity measurements indicated by $\underline{\alpha}$, $\underline{y_b}$ and $\underline{y_e}$ can be defined as

$$\underline{y_b} = \begin{bmatrix} \underline{m_b} & \underline{\alpha_b} \end{bmatrix}^T \tag{3.4}$$

$$\underline{y_e} = \begin{bmatrix} \underline{m_e} & \underline{\alpha_e} \end{bmatrix}^T \tag{3.5}$$

where M is defined as shown in Equation (3.6).

$$M = \begin{bmatrix} R_b^e & 0 \\ 0 & R_b^e \end{bmatrix} \tag{3.6}$$

The attitdue determination algorithm seeks to minimize the error by estimating the quaternion that best expresses the rotation between the body frame the navigation frame, where the quaternion is written as shown in Equation (3.7).

$$n = a\hat{i} + b\hat{j} + c\hat{k} + d \tag{3.7}$$

This means that R_b^e can be rewritten as shown below.

$$R_b^e = \begin{bmatrix} d^2 + a^2 - b^2 - c^2 & 2(ab - cd) & 2(ac + bd) \\ 2(ab + cd) & d^2 + b^2 - a^2 - c^2 & 2(bc - ad) \\ 2(ac - bd) & 2(bc + ad) & d^2 + c^2 - b^2 - a^2 \end{bmatrix} \tag{3.8}$$

With R_b^e in terms of the quaternion components, a Gauss-Newton iterative process can be used to estimate the terms in the quaternion n through the Jacobian matrix J such that

$$\hat{n}_{k+1} = \hat{n}_k - [J^T(\hat{n}_k)J(\hat{n}_k)]^{-1}J^T(\hat{n}_k)\epsilon(\hat{n}_k) \tag{3.9}$$

where

$$J = \begin{bmatrix} \frac{\delta M}{\delta a} \underline{y}_b & \frac{\delta M}{\delta b} \underline{y}_b & \frac{\delta M}{\delta c} \underline{y}_b & \frac{\delta M}{\delta d} \underline{y}_b \end{bmatrix} \quad (3.10)$$

$$\epsilon(\hat{n}_k) = \underline{y}_e - M(\hat{n}_k)\underline{y}_b \quad (3.11)$$

By iterating Equation (3.9) until convergence, the quaternion rotation that minimizes the error function in Equation (3.3) will be found. Using this quaternion, the rotation matrix in Equation (3.8) can be calculated. If necessary, the rotation matrix can also be converted back to Euler angles.

3.3 Simulated Vehicle Attitude Determination

To test the AHRS presented in the previous section, a simulated vehicle trajectory was created using a vehicle dynamic model. The model was put through a series of turns and accelerations with zero pitch and roll to test the attitude determination algorithm. Based off of the model, sensor measurements for the accelerometer and magnetometer could be generated by using the noise characteristics of an Xsens IMU shown in Table 3.1. The simulated path is shown in Figure 3.2 in a North-East-Down (NED) navigation frame along with the vehicle velocity and heading in Figures 3.3 - 3.4, followed by the attitude estimates and errors in Figures 3.5 - 3.7.

Table 3.1: Xsens Error Characteristics

Measurement	Standard Deviation	Bias Standard Deviation
Acceleromter (m/s^2)	0.0098	0.0333
Gyroscope (rad/s)	$8.7266x10^-4 - 10^-3$	0.0014
Magnetometer $(mGauss)$	0.5	-

Overall, the AHRS performs very well, with the error being approximately +/- two degrees on all axes. However, when the vehicle makes sudden turns or accelerations, the error spikes. The change represents a step input, and the spikes are the transient response
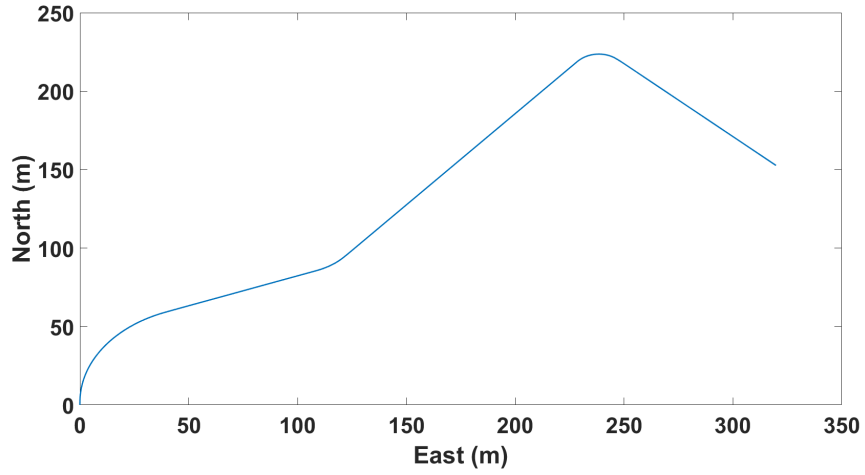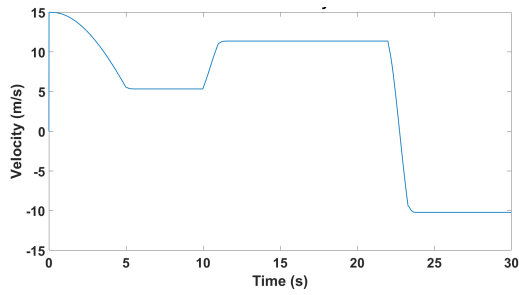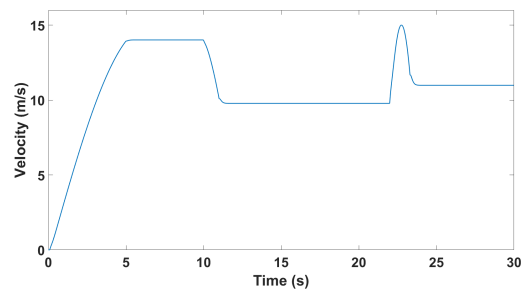
Figure 3.2: Simulated Vehicle Trajectory
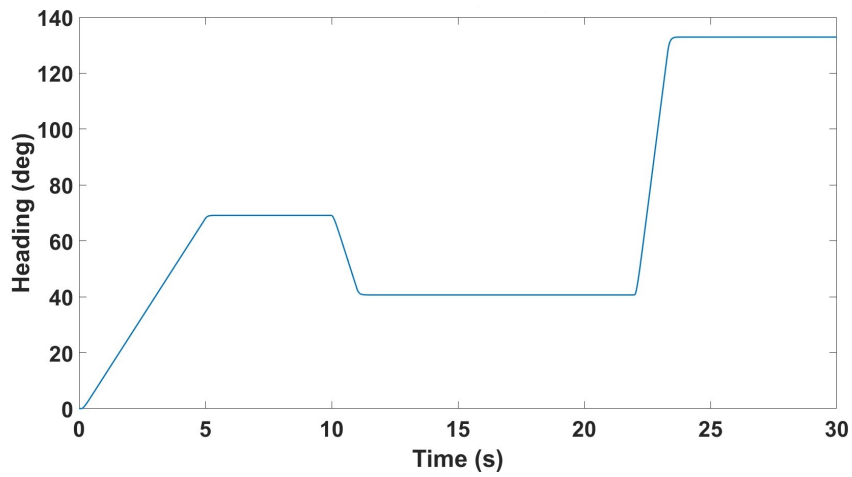

(a) North Velocity

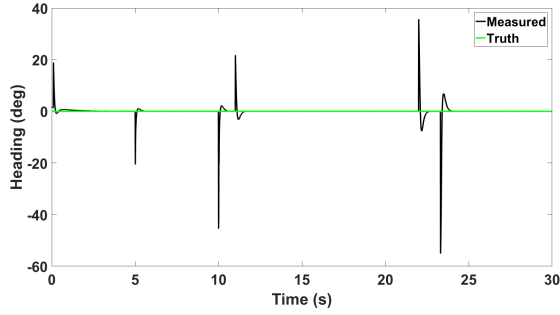(b) East Velocity

Figure 3.3: Simulated Vehicle Velocity

Figure 3.4: Simulated Vehicle Heading

(a) Roll
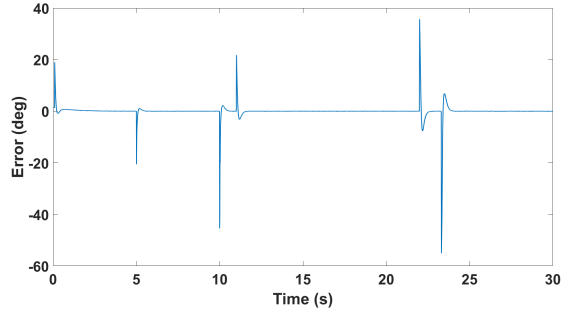
(b) Roll Error
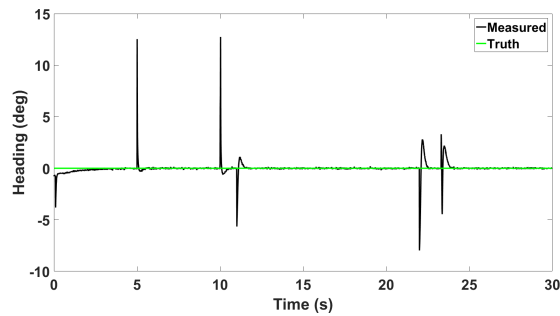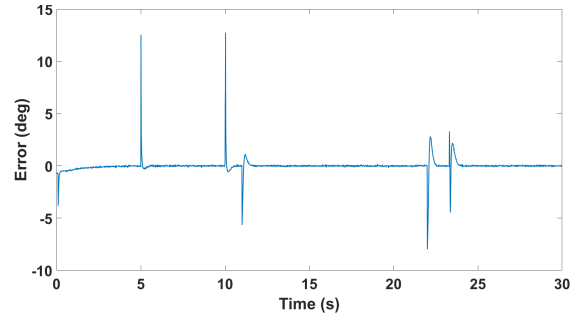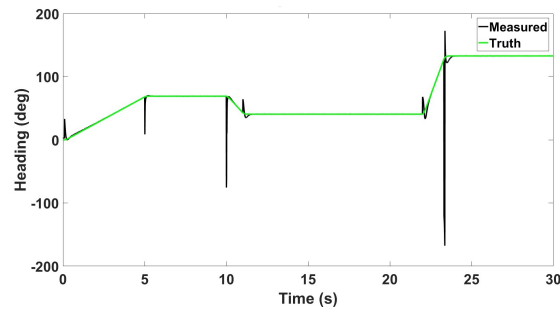
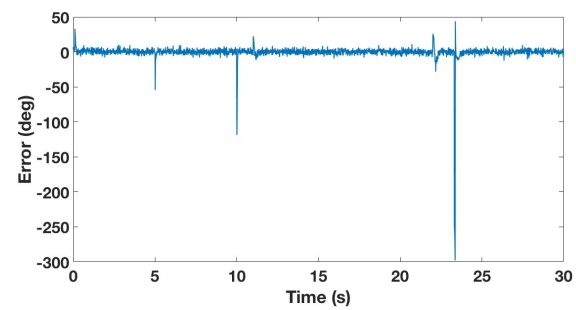Figure 3.5: Simulated Vehicle Roll

(a) Pitch

(b) Pitch Error

Figure 3.6: Simulated Vehicle Pitch

(a) Heading

(b) Heading Error

Figure 3.7: Simulated Vehicle Heading

of the AHRS. This error occurs because the algorithm is attempting to match the measured acceleration with the gravity vector. The problem with this comparison will be discussed in more detail in Section 3.5.

3.4 Experimental Attitude Determination

After the attitude determination algorithm was verified in simulation, it was tested experimentally. The Infiniti G35 was driven in a circular path similar to what was used for the magnetometer calibration, except now the accelerometer and the magnetometer data from the Xsens are used to calculate roll, pitch, and yaw, and the the three-antenna Septentrio is used as the reference for attitude truth. Figures 3.8 - 3.10 show the measured and true vehicle attitude, along with the error in attitude between the attitude determination algorithm and the Septentrio measured attitude. The experimental data confirms that this algorithm can accurately calculate the attitude of a vehicle. Roll and pitch errors are never more than five degrees, and usually less then three degrees. The heading error appears to suffer from a constant bias of approximatley three to four degrees, likely due to misalignment between the IMU and the GPS antennas. If this bias was accounted for, the heading error would be mostly within five degrees.

3.5 Conclusions

This chapter provided a review of several attitude determination algorithms, and outlined the process and relevant equations for the AHRS used in the rest of this thesis. The algorithm selected was then verified through both simulation and experimental data. However, there is one inherent flaw in this algorithm. The chosen algorithm for calculating
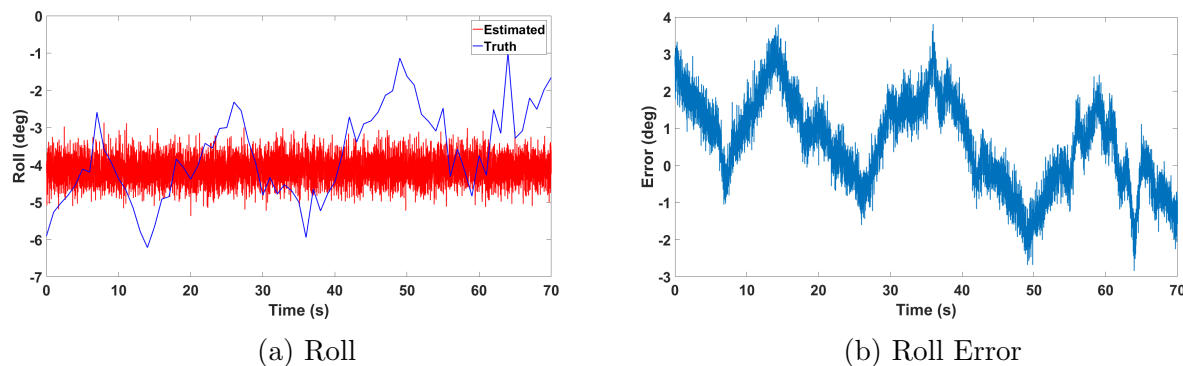

(a) Roll   (b) Roll Error

Figure 3.8: Vehicle Roll with Experimental Data

(a) Pitch

(b) Pitch Error
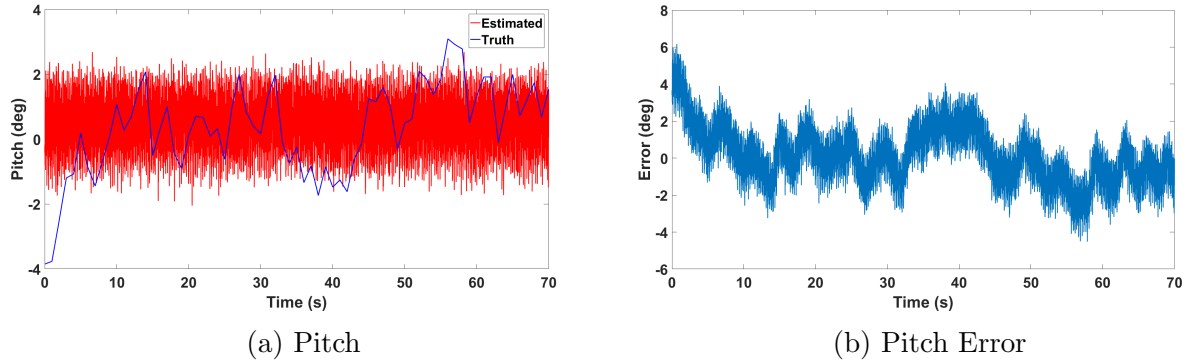
Figure 3.9: Vehicle Pitch with Experimental Data

(a) Heading

(b) Heading Error
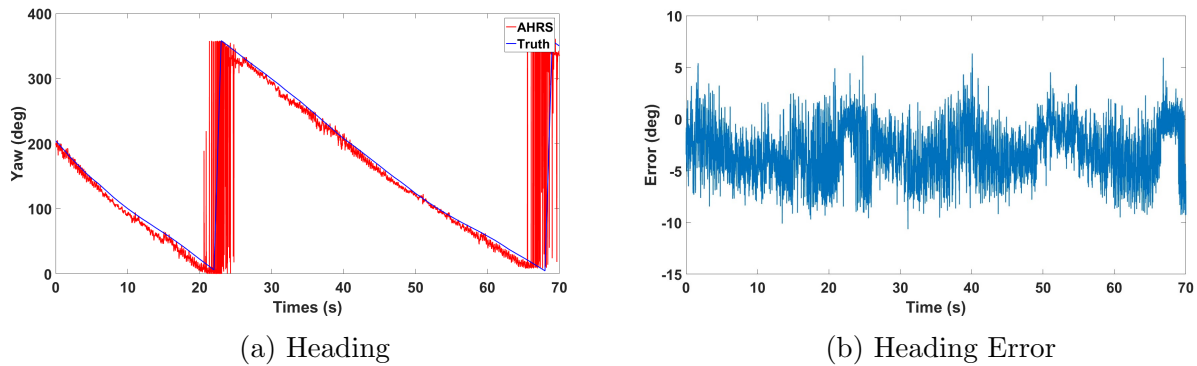
Figure 3.10: Vehicle Heading with Experimental DataNoTitle

attitude attempts to find a rotation matrix that matches magnetometer data to an earth magnetic field model, and accelerometer data to a gravity model. The issue here arises when a vehicle experiences large amounts of acceleration. For the algorithm to work perfectly, the accelerometer must be measuring only gravity. However, in any realistic scenario, the vehicle will be accelerating in some manner. In principle, this means the attitude calculation will have errors. In this chapter, the simulation had various accelerations, both linear and centripetal and was still able to calculate an accurate attitude estimate. The experimental data had one continuous centripetal acceleration and many other accelerations caused by the rough, offroad path of the vehicle during data collection. Although these non-gravitational accelerations cause a large amount of noise in the attitude estimate, the attitude determination algorithm was still able to calculate the vehicle's attitude. Some of the work done

in [36] also shows how the algorithm breaks down under extreme, multiple-gravity accel-
erations. However, the majority of consumer vehicles will never approach those levels of
continuous accelerations, so it is not a concern for this thesis. One option to eliminate the
acceleration errors is to use velocity vectors [36]. A wheel encoder can measure the vehicle
velocity, while a global measurement of velocity, usually provided by GPS, can be used as
another measurement of velocity. Since the purpose of this thesis is to avoid using GPS,
this method was not used. Another option could be used if the vehicle dynamic model is
well-known. Using the vehicle model, non-gravity measurements of the accelerometer could
be removed, however this method was not explored in this thesis and is left for future work.

Chapter 4

Covariance Analysis of INS Propagation

As IMUs continue to become cheaper and smaller, their popularity for use in navigation increases. From planes to ships to cell phones, IMUs are easily incorporated into most integrated circuits, and provide high-frequency updates on acceleration and angular rates. This size and cost reduction is especially important in the race to mass-produce the first autonomous consumer vehicle. However, creating technology that is both cheaper and smaller is not without drawbacks. To keep an IMU's cost below the thousands of dollars required for high precision, tradeoffs are made in noise and stability. Many consumer IMUs suffer from bias and drift, and when utilized in an inertial navigation system (INS) to form position, velocity, and attitude (PVA) estimates, the solution will quickly drift off track with unbounded error. There are ways of correcting IMU errors, such as step detection in pedestrian dead-reckoning [39], or using GPS measurements in an Extended Kalman Filter (EKF) [21, 41]. However, the goal of this thesis is to show that IMUs can be paired with other measurements, namely range and attitude, to bound the error that comes with integrating and propagating IMU measurements. In the following sections, INS navigation will be discussed with detailed analysis on unaided and radar/attitude aided INS.

4.1 INS Propagation Model

The process of propagating an INS can be done by using Equations (4.1 - 4.5), which are derived from [21].

$$\hat{R}_{b,k+1}^{n} = \hat{R}_{b,k}^{n}(I_{33} + \Omega_{ib}dt) \tag{4.1}$$

$$\Omega_{ib} = [(\omega_k - \hat{b}_{g,k}) \wedge] \tag{4.2}$$

$$f_{ib}^n = \frac{1}{2}(\hat{R}_{b,k+1}^n + \hat{R}_{b,k}^n)(\alpha_k - \hat{b}_{a,k}) \tag{4.3}$$

$$\hat{V}_{k+1} = \hat{V}_k + (f_{ib}^n + g_n)\Delta t \tag{4.4}$$

$$\hat{P}_{k+1} = \hat{P}_k + \frac{\Delta t}{2}(\hat{V}_{k+1} + \hat{V}_k) \tag{4.5}$$

The outputs of interest are the rotation matrix, $\hat{R}_{b,k+1}^n$, the velocity, $\hat{V}_{k+1}$, and the position, $\hat{P}_{k+1}$. The current gyroscope measurement is represented by ω_k. The current accelerometer measurement is represented by α_k. The IMU time step between measurements is represented by Δt, and the two bias terms come from the values in the error state vector of the previous iteration. The error state vector is given below in Equation 4.6.

$$\hat{x} = \begin{bmatrix} \delta P & \delta V & \delta \Psi & b_a & b_g \end{bmatrix}^T \tag{4.6}$$

In Equation (4.2), the '$\wedge$' symbol indicates a skew symmetric matrix, and in Equation (4.4), g_n is the gravity vector in the local navigation frame. An error state vector is chosen as it keeps the estimates small, and reduces errors from linearization of the dynamic equatiuons [21, 40]. Since the INS is unaided with no external measurements, its propagation can be represented as an Extended Kalman Filter without a measurement update

$$\hat{x}_{k+1}^- = \hat{x}_k^+ + \Phi_{k+1}\hat{x}_k^+ \tag{4.7}$$

$$P_{k+1}^- = \Phi_{k+1}P_k^+\Phi_{k+1}^T + B_wQB_w^T \tag{4.8}$$

where $\hat{x}$ is the vector of the estimates of the state, P is the state estimate error covariance matrix, and Φ_{k+1} is the truncated matrix exponential approximated below.

$$\Phi_{k+1} = I + F_{k+1}\Delta t \tag{4.9}$$

F is the system model matrix, which is constructed by taking the partial derivatives of the following equations with respect to $\hat{x}$.

$$\delta \dot{P} = \delta V \tag{4.10}$$

$$\delta \dot{V} = R_b^n(\alpha - b_a) - g_n \tag{4.11}$$

$$\delta \dot{\Psi} = R_b^n(\omega - b_g) \tag{4.12}$$

Since the IMU biases are included in the state, it is necessary to have the appropriate model equations for them. For this work, the IMU biases are modeled as a first order Markov process as shown in Equation (4.13).

$$\dot{b} = -\frac{1}{\tau}b + \mu \tag{4.13}$$

When the partial derivative with respect to the state vector is taken, Equations (4.10 - 4.13) will yield the system dynamics model, F,

$$F = \begin{bmatrix} O_{33} & I_{33} & O_{33} & O_{33} & O_{33} \\ O_{33} & O_{33} & [(R_b^n\underline{\alpha})\wedge] & R_b^n & O_{33} \\ O_{33} & O_{33} & O_{33} & O_{33} & R_b^n \\ O_{33} & O_{33} & O_{33} & -\frac{1}{\tau_a}I_{33} & O_{33} \\ O_{33} & O_{33} & O_{33} & O_{33} & -\frac{1}{\tau_g}I_{33} \end{bmatrix} \tag{4.14}$$

where I_{33} represents a 3x3 identity matrix, and O_{33} represents a 3x3 matrix of zeros. This matrix can now be used to propagate the error-state estimates by using Equations (4.7) and (4.9), and the error covariance matrix, P, is propagated with Equation (4.8). The error covariance matrix depends on the process noise covariance matrix, Q, and the system model noise sources, B_w, which are given by the following equations

$$
Q = \begin{bmatrix} \sigma_a^2 & 0_{33} & 0_{33} & 0_{33} \\ 0_{33} & \sigma_g^2 & 0_{33} & 0_{33} \\ 0_{33} & 0_{33} & \sigma_{ba}^2 & 0_{33} \\ 0_{33} & 0_{33} & 0_{33} & \sigma_{bg}^2 \end{bmatrix} \tag{4.15}
$$

$$
B_w = \begin{bmatrix} 0_{33} & 0_{33} & 0_{33} & 0_{33} \\ R_b^e & 0_{33} & 0_{33} & 0_{33} \\ 0_{33} & R_b^e & 0_{33} & 0_{33} \\ 0_{33} & 0_{33} & R_b^e & 0_{33} \\ 0_{33} & 0_{33} & 0_{33} & R_b^e \end{bmatrix} \tag{4.16}
$$

where each σ^2 term is a 3x3 diagonal matrix representing the variance on the corresponding process noise source. Although these values are a tuning parameter, a good inital starting point is the reported variances of the accelerometer and gyroscope measurements. Also in this thesis, P was always initialized as an identity matrix.

A way of measuring the effectiveness of an estimator is to analyze the state estimate error covariance matrix, P. This matrix is essentially a measure of the "uncertainty" of the estimates. For a good estimator, the diagonals of the covariance matrix will be bounded. To examine the uncertainty of navigation estimates through IMU propagation, a simple simulation was run of a VectorNav300 IMU, shown in Figure 4.1. The IMU was simulated moving in a straight line at a constant velocity, then integrated and propagated using the previously described process. To demonstrate how INS aiding can reduce errors associated with IMU propagation, two different scenarios were examined. The first scenario is the unaided INS, the second scenario being radar and attitude aided INS. The error characteristics of the VectorNav300 and a Delph ESR, shown in Table 4.1, were used in the Q and R matrices, and the P matrix was intialized as an identity matrix.

Table 4.1: Standard Deviations of VectorNav300 and Delphi ESR Measurements

Sensor	Measurement (m/s^2)	Standard Deviation (rad/s)
VectorNav300	Acceleration	$.00014 * \sqrt{50}\ m/s^2$
VectorNav300	Angular Rate	$.0035 * \sqrt{50} * \frac{\pi}{180}\ rad/s$
Delphi ESR	Range	$.5\ m$
Delphi ESR	Range Rate	$.12\ m/s$
Delphi ESR	Azimuth	$.5 * \frac{\pi}{180}\ rad$

Figure 4.1: VectorNav 300 IMU

4.2 Unaided INS

Since the unaided INS has no measurement update, there is no way to correct the estimates and keep error constrained. This means that an unaided INS will have an ever-increasing uncertainty. This turns out to be the case, as can be seen in Figure 4.2. Although the plot is only for the estimate of North position, the other states behave in the same manner. This unbounded growth in uncertainty shows why it is necessary for an INS to be coupled with some form of measurement.

4.3 Fully Aided INS

Next, the INS was aided with radar and attitude measurements. The goal of adding these measurements is to constrain the error so that the covariance does not grow unbounded as it does in the unaided case. With the addition of measurements to the INS, a measurement update must now be applied to the propagation equations. The following section will detail the equations used in the measurement update of the Extended Kalman Filter.
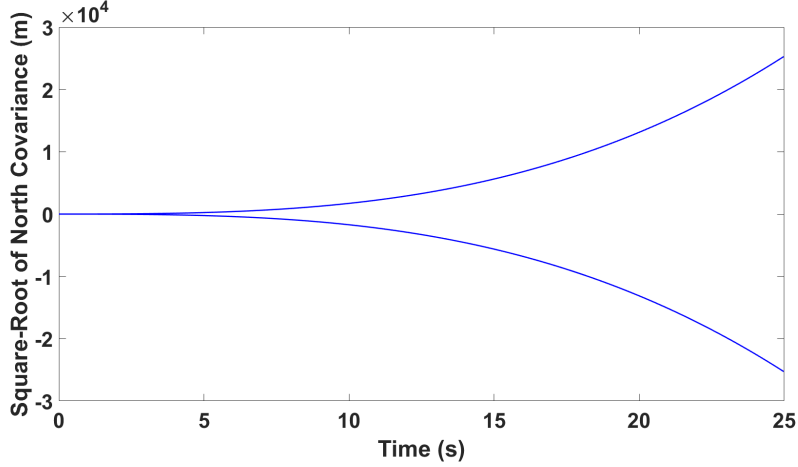
Figure 4.2: Unaided INS North Covariance

4.3.1 Measurement Update Equations

Previously, the equations for INS navigation were introduced as an Extended Kalman Filter without a measurement update. However, when radar and attitude measurements are added, then the filter may now include a measurement update. The three equations that make up the measurement update are defined as

$$L_{k+1} = P_{k+1}^- H_{k+1}^T (H_{k+1} P_{k+1}^- H_{k+1}^T + R)^{-1} \tag{4.17}$$

$$P_{k+1}^+ = (I - L_{k+1} H_{k+1}) P_{k+1}^- \tag{4.18}$$

$$\hat{x}_{k+1}^+ = \hat{x}_{k+1}^- + L_{k+1} \delta z_{k+1} \tag{4.19}$$

where a '+' denotes a value calculated in the measurement update, a '−' symbol denotes a value calculated in the time update, L is the Kalman Gain, H is the measurement Jacobian matrix that maps the measurements to the states, and δz is the difference between the actual measurements and the predicted measurements. Ideally, there are six possible measurements a radar can return, as defined by the following equations given by [27].

$$R = \sqrt{\Delta X^2 + \Delta Y^2 + \Delta Z^2} \tag{4.20}$$

$$\dot{R} = \frac{\Delta X \Delta \dot{X} + \Delta Y \Delta \dot{Y} + \Delta Z \Delta \dot{Z}}{\sqrt{\Delta X^2 + \Delta Y^2 + \Delta Z^2}} \tag{4.21}$$

$$\lambda_y = \tan^{-1}\left(\frac{\Delta Y}{\Delta X}\right) \tag{4.22}$$

$$\lambda_z = \tan^{-1}\left(\frac{\Delta Z}{\Delta X}\right) \tag{4.23}$$

$$\dot{\lambda}_y = \frac{\Delta X \Delta \dot{Y} - \Delta Y \Delta \dot{X}}{\Delta X^2 + \Delta Y^2} \tag{4.24}$$

$$\dot{\lambda}_z = \frac{\Delta X \Delta \dot{Z} - \Delta Z \Delta \dot{X}}{\Delta X^2 + \Delta Z^2} \tag{4.25}$$

These are the measurement equations for range, range rate, azimuth, elevation, azimuth rate, and elevation rate, respectively. Here, $\Delta X, \Delta Y$, and ΔZ are the difference between the radar's position and the target's position in the navigation frame. In this thesis, the radar's position was assumed to be on a non-moving ground station at $(0, 0, 0)$. In this case, each delta term simplifies to just X, Y, and Z, and $\dot{X}$, $\dot{Y}$, and $\dot{Z}$, which correspond to the vehicle's position and velocity in the navigation frame. Also, the radar was positioned so that it was facing due north, and it was assumed that the radar was level in the navigation frame. Most radars cannot provide all six measurements, and may only report range, range rate, and azimuth. In this thesis, a Delphi ESR, shown in Figure 4.3, is one such radar that only reports range, range rate, and azimuth. This results in a measurement vector as shown below in Equation (4.26).

$$z = \begin{bmatrix} \lambda_y & R & \dot{R} & \phi & \theta & \psi \end{bmatrix} \tag{4.26}$$

38

Figure 4.3: Delphi ESR

H is a Jacobian of the measurement vector, so by taking the partial derivatives of z with respect to the states, the rows for H can be defined as follows

$$H_1 = \begin{bmatrix} \frac{-Y}{X^2+Y^2} \\ \frac{X}{X^2+Y^2} \\ 0_{13,1} \end{bmatrix}^T \tag{4.27}$$

$$H_2 = \begin{bmatrix} \frac{X}{\sqrt{X^2+Y^2+Z^2}} \\ \frac{Y}{\sqrt{X^2+Y^2+Z^2}} \\ \frac{Z}{\sqrt{X^2+Y^2+Z^2}} \\ 0_{12,1} \end{bmatrix}^T \tag{4.28}$$

$$H_3 = \begin{bmatrix} \frac{\dot{X}}{\sqrt{X^2+Y^2+Z^2}} - \frac{X(X\dot{X}+Y\dot{Y}+Z\dot{Z})}{(X^2+Y^2+Z^2)^{3/2}} \\ \frac{\dot{Y}}{\sqrt{X^2+Y^2+Z^2}} - \frac{Y(X\dot{X}+Y\dot{Y}+Z\dot{Z})}{(X^2+Y^2+Z^2)^{3/2}} \\ \frac{\dot{Z}}{\sqrt{X^2+Y^2+Z^2}} - \frac{Z(X\dot{X}+Y\dot{Y}+Z\dot{Z})}{(X^2+Y^2+Z^2)^{3/2}} \\ \frac{X}{\sqrt{X^2+Y^2+Z^2}} \\ \frac{Y}{\sqrt{X^2+Y^2+Z^2}} \\ \frac{Z}{\sqrt{X^2+Y^2+Z^2}} \\ 0_{9,1} \end{bmatrix}^T \tag{4.29}$$

$$H_4 = \begin{bmatrix} 0_{33} \\ 0_{33} \\ I_{33} \\ 0_{33} \\ 0_{33} \end{bmatrix}^T \tag{4.30}$$

and H is defined as

$$H = \begin{bmatrix} H_1 \\ H_2 \\ H_3 \\ H_4 \end{bmatrix} \tag{4.31}$$

which will result in a (6x15) measurement matrix. With the state vector defined and the measurement sources known, the measurement covariance matrix can be defined as

$$R = \begin{bmatrix} \sigma_{\lambda_y}^2 & 0 & 0 & 0_{13} \\ 0 & \sigma_R^2 & 0 & 0_{13} \\ 0 & 0 & \sigma_{\dot{R}}^2 & 0_{13} \\ 0_{31} & 0_{31} & 0_{31} & \sigma_{\Psi}^2 \end{bmatrix} \tag{4.32}$$

where the first three terms on the diagonal are the variances for the range, range rate, and azimuth measurements as given by Table 4.1, and the last term on the diagonal is the 3x3 matrix of the variances on the attitude estimates from the AHRS which was initialized as .01 deg^2. After the measurement update is complete, the position, velocity, and attitude estimates must be updated using the error-state estimates.

$$\hat{P}_{k+1} = \hat{P}_k + \delta P \tag{4.33}$$

$$\hat{V}_{k+1} = \hat{V}_k + \delta V \tag{4.34}$$

$$\hat{\Theta}_{k+1} = \delta\Psi \tag{4.35}$$

$$\hat{R}^n_{b,k+1} = \hat{R}^n_{b,k}(2I_{33} + \Theta_{k+1})/(2I_{33} - \Theta_{k+1}) \tag{4.36}$$

The updated estimate for attitude can be obtained by decomposing the transpose of $\hat{R}^n_{b,k+1}$. After the PVA estimates are updated, the error-state vector is reset to zero and the process is repeated. A block diagram of the Extended Kalman Filter process is shown in Figure 4.4.
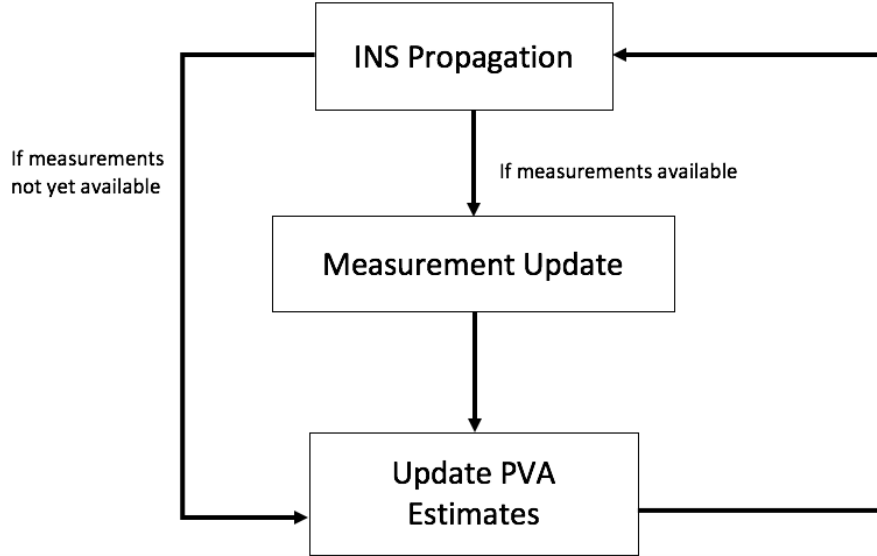

Figure 4.4: Diagram of the Extended Kalman Filter Filter Process

One limitation in this filter structure lies in how the accelerometer measurements are used. In the time update, the accelerometer is used to propagate the states. In the measurement update, the acceleration is used in the attitude estimates through the AHRS. This

41

causes some terms in the Q and R matrices to become correlated. An important assumption of the Kalman filter is that Q and R are uncorrelated. This problem is discussed in greater detail in Appendix B.

4.3.2 Fully Aided Covariance

As shown previously, without any external measurements, INS propagation will result in unbounded error growth. In the previous section, a measurement update was been added that aids the INS with radar range, range rate, and azimuth as well as AHRS attitude estimates. This results in a bounded uncertainty, as shown in Figure 4.5. These results show that a radar and attitude aided INS filter is stable and should be able to return an acurrate navigaiton solution. To validate the results of this chapter, the described filter will be tested in simulation in Chapter 5.
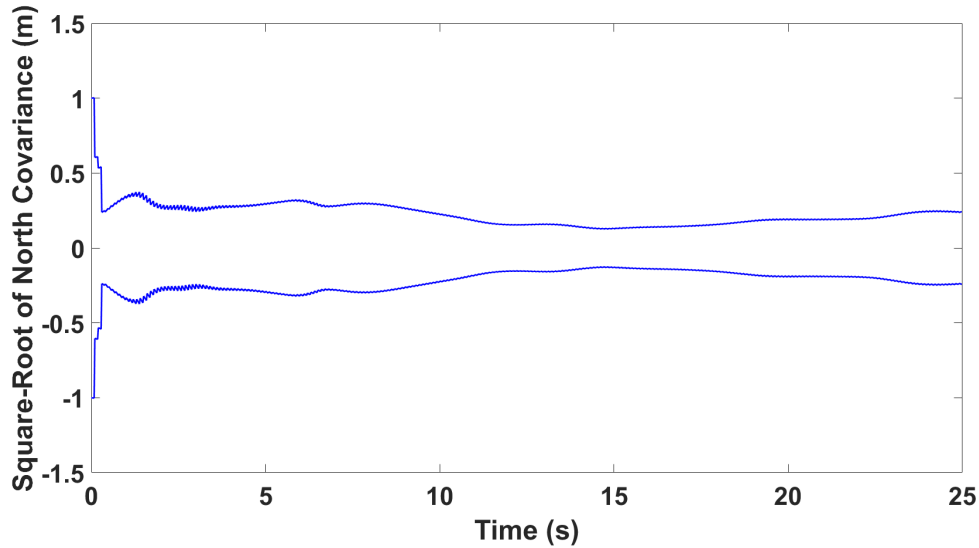
Figure 4.5: Fully Aided INS North Covariance

4.4 Conclusions

In this chapter, the concept of INS navigation was introduced and the equations used for INS propagation were given. Due to the errors present in IMUs, it was shown that

measurements from other sensors are necessary to bound the errors that occur with pure INS navigation. The state estimate error covariance matrix was also introduced with examples to show how it can be used as a metric for judging if a filter will return a good navigation solution. Without any aiding, it was shown that the estimate uncertainty grows unbounded, and no navigation solution can be formed. Next, the defining equations for radar were given along with the equations for a Kalman Filter measurement update. It was then shown how radar and attitude measurements can be used to aid an INS through the Extended Kalman Filter structure. It was also shown that by aiding the INS with radar and attitude, the estimate uncertainty can be bounded, which results in a good navigation solution. The resulting radar-aided INS will be further discussed and tested in Chapter 5.

Chapter 5

Radar-Aided INS Filter

As shown in the previous chapters, magnetometers and accelerometers can be very useful for vehicle heading and attitude determination, however in navigation it is often required that a vehicle's position and velocity also be estimated. To do this, IMUs and GPS are commonly coupled together in navigation filters. The reasoning behind this is that IMUs and GPS are complementary; where one may fall short, the other stands strong. IMUs typically have a very high update rate and can estimate position, velocity, and attitude (PVA). Despite the advantage of fast PVA estimates, IMUs suffer from bias and other errors, which will cause the solution to rapidly drift from truth if no corrections are provided.

In contrast to the IMU, GPS has a much slower update rate, but can provide position and velocity measurements with long-term accuracy and stability. When GPS measurements are paired with an IMU, the INS can continue to provide navigation solutions until GPS measurements are re-acquired, and while GPS measurements are being received, the IMU errors can be corrected to ensure the accuracy of the INS. However, GPS measurements are subject to outages caused by faulty measurements or blockages from structures or terrain. The goal of this thesis is to propose a potential alternative to the commonly used GPS/INS navigation filter. This is accomplished by combining radar measurements with an inertial navigation system, in what has been dubbed a radar-aided INS navigation filter, or a RAINS filter. By itself, a radar does not yield enough measurements to estimate a vehicle's position, velocity, and attitude. This is where the importance of an attitude measurement comes in. As discussed previously, a magnetometer can be calibrated and combined with another vector sensor, such as an accelerometer, to form an attitude heading reference system. When GPS measurements in a navigation filter are replaced with radar measurements, an attitude
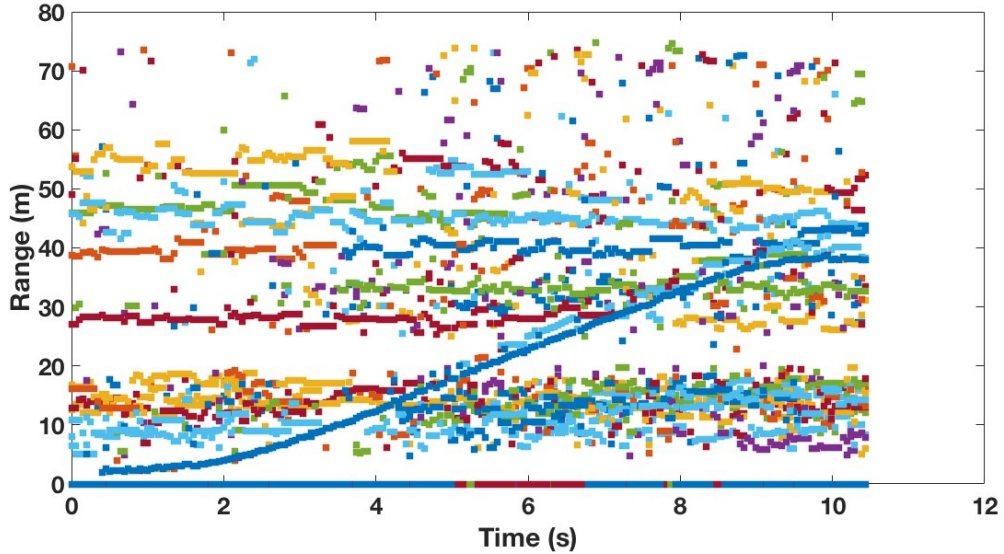
Figure 5.1: Delphi Range Measurements with No Filtering

measurement is required or else the RAINS filter's estimates will diverge, as radar does not provide enough measurements to estimate a vehicle's attitude. When the RAINS filter has attitude measurements, it can successfully correct dead-reckoning errors and constrain PVA errors.

5.1 Radar Target Determination

When radar signals are reflected back from an object, there is no way to know for certain whether the signal is returning from a valid target, or clutter in the environment. For this reason, target determination is imperative to make sure the radar measurements are accurate and also represent the correct target. The Delphi ESR uses 64 channels, which means at each measurement time, there can be up to 64 different measurements on range, range rate and azimuth. The output from the Delphi will look similar to what is shown in Figure 5.1.

The true range measurements are completely crowded out by clutter, which is what makes target determination so important. There are statistical target acquistion methods available for reducing clutter [6]. However, that level of target acquisition was outside the scope of this thesis and has been left for future work. In this thesis, simple filtering methods
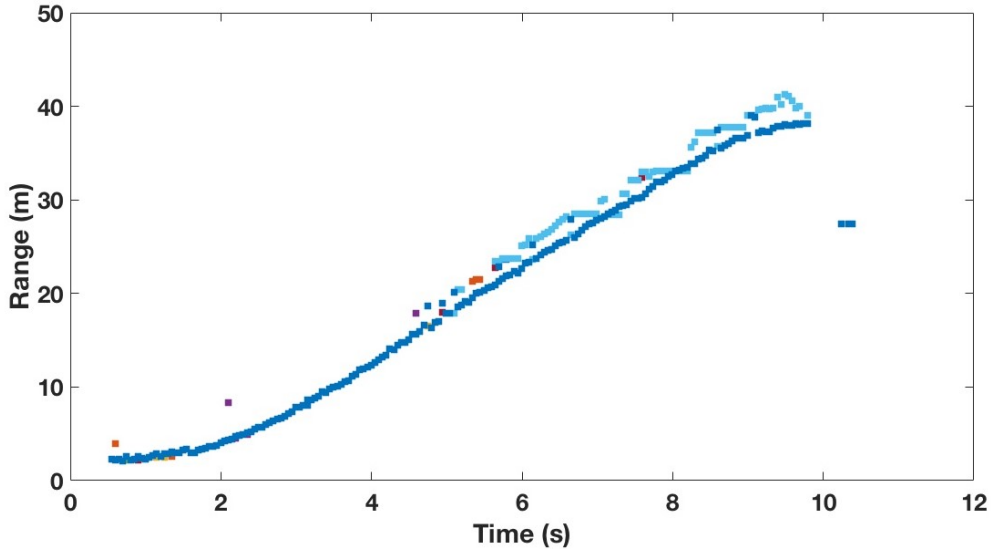
Figure 5.2: Delphi Range Measurements with Filtering

were used instead. First, all radar measurements on the Delphi are returned with a status message that represents the trustworthiness of the measurements. A status of '0' indicates that the Delphi has determined that channel is not tracking a valid target, and can be removed. Second, some intuition can be used to filter out more clutter. For instance, it is known that the vehicle path will never be greater than a certain range, and the vehicle's speed will never be over a certain rate. This is very analogous to a radar operating on a road where the max distance the radar is being used to track a vehicle and speed limits on the road would set a gate for what range and range rates are to be expected. Using this simple radar data clustering technique, the raw measurements in Figure 5.1 can be filtered and reduced down to what is shown in Figure 5.2.

Although not all erroneous measurements will be removed, the filter removes much of the clutter, and will greatly improve the measurements of the target. After filtering, the average measurement at each time can be taken to produce a measurement that can be used in the RAINS filter. This results in radar range measurements similar to what is shown in Figure 5.3, along with corresponding range rate and azimuth.
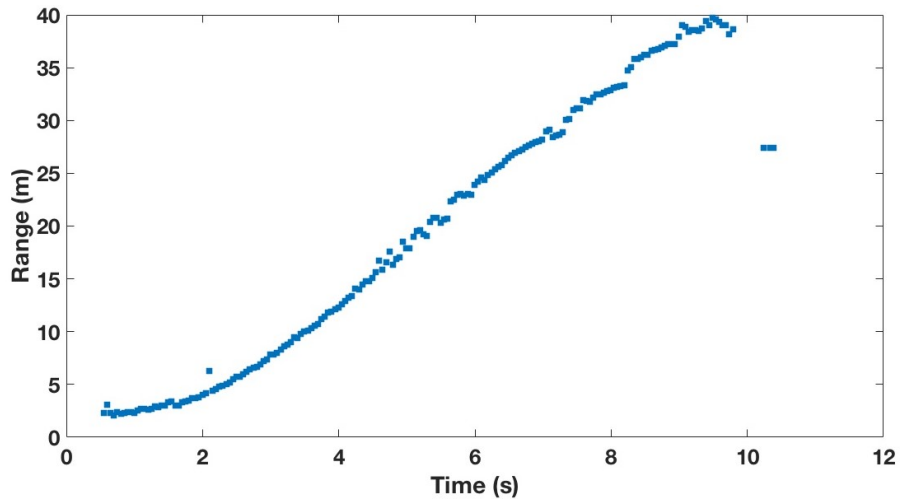
(a) Average Range After Filtering
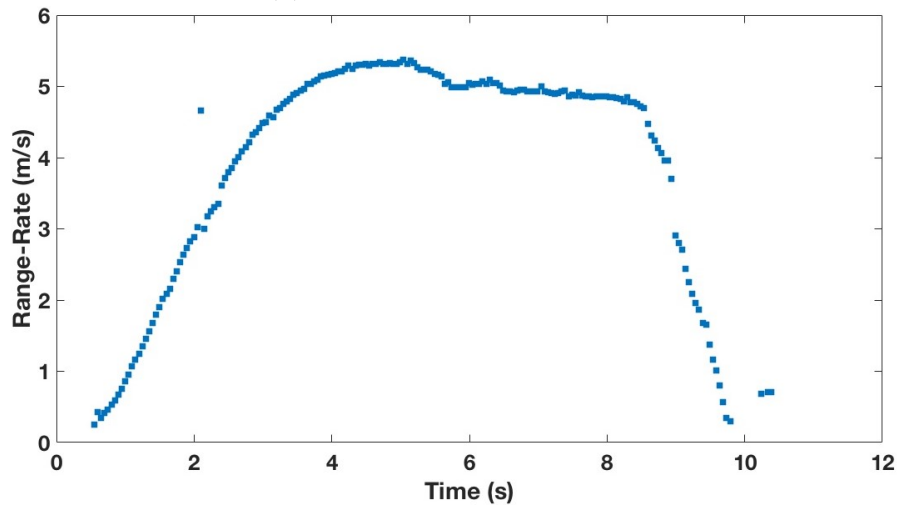
(b) Average Range Rate After Filtering
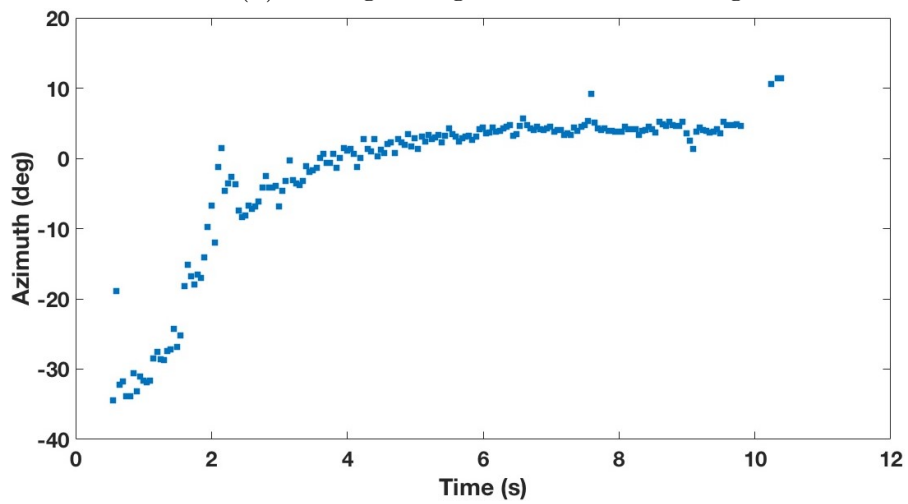
(c) Average Azimuth After Filtering

Figure 5.3: Average Radar Measurements After Filtering

As can be seen, even simple filtering techniques can be useful for reducing clutter and calculating a good estimate for the radar measurements on the target. As stated earlier, statistical filtering was beyond the scope of this work, but for a good example of how it can be used to improve clutter reduction, especially when tracking a target on a less predictable path, see [43].

5.2 Simulation Results

To test the RAINS filter in simulation, a vehicle trajectory was created in MATLAB. By using the performance and error characteristics of the VectorNav 300 IMU and the Delphi ESR as shown in Table 5.1, sensor measurements were generated and an attitude estimate was made using the AHRS described in Chapter 3. The values in the Q matrix were initialized by using the VectorNav error characteristics, the values in the R matrix were set as the variances on the Delphi measurements, while the variance on attitude was initialized at .01 deg^2. The true vehicle path is shown in Figures 5.4 - 5.6, and the estimator results are shown in Figures 5.7 - 5.13.

Table 5.1: Standard Deviations of VectorNav 300 and Delphi ESR Measurements

Sensor	Measurement (m/s^2)	Standard Deviation (rad/s)
VectorNav 300	Acceleration	$.00014 * \sqrt{50} \ m/s^2$
VectorNav 300	Angular Rate	$.0035 * \sqrt{50} * \frac{\pi}{180} \ rad/s$
Delphi ESR	Range	$.5 \ m$
Delphi ESR	Range Rate	$.12 \ m/s$
Delphi ESR	Azimuth	$.5 * \frac{\pi}{180} \ rad$

As seen in Figure 5.7, the dead-reckoning solution drifts quickly to the point of becoming completely unusable for PVA estimates on its own. Despite the drift from the IMU, Figure 5.7 also shows that the RAINS filter is able to overcome those errors and correctly estimate position. Figure 5.8 shows the error is within five meters of truth. Similar results are achieved with velocity and attitude. Despite large the amounts of drift from dead reckoning on velocity shown in Figures 5.9 and 5.10, the RAINS filter is able to accurately estimate
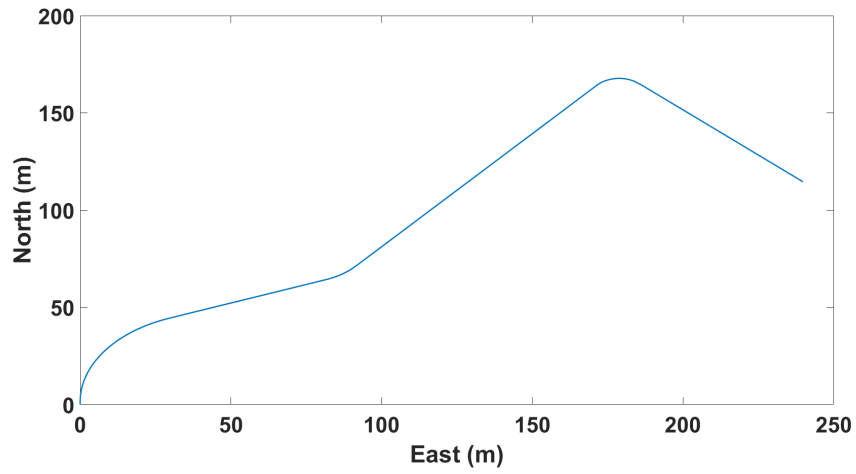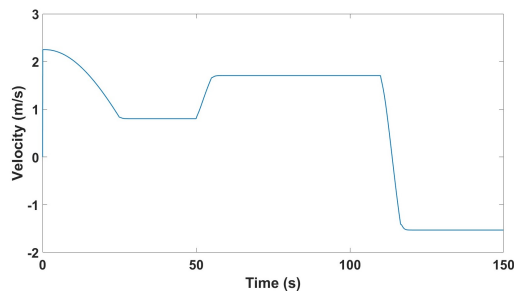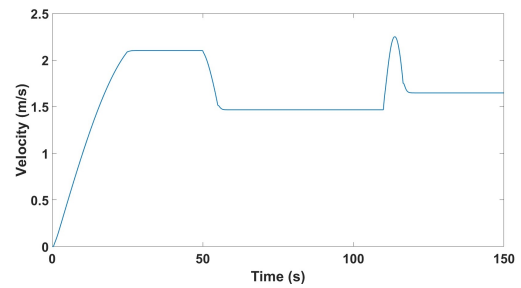
Figure 5.4: Simulated Vehicle Trajectory

(a) North Velocity

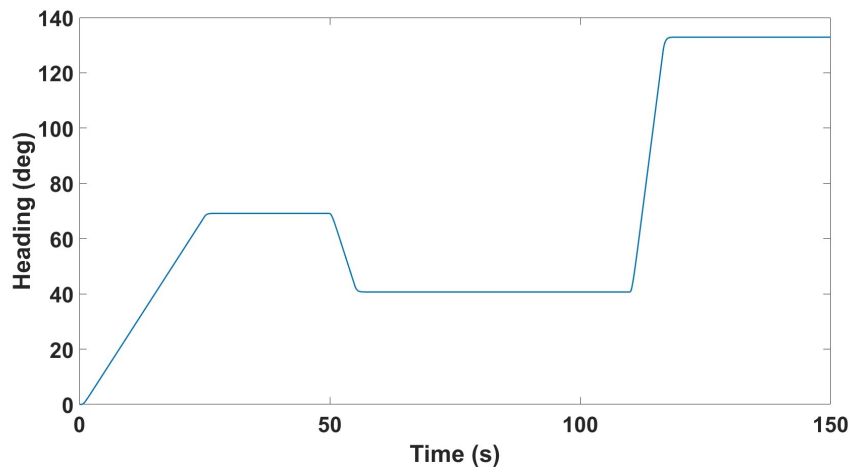(b) East Velocity

Figure 5.5: Simulated Vehicle Velocity

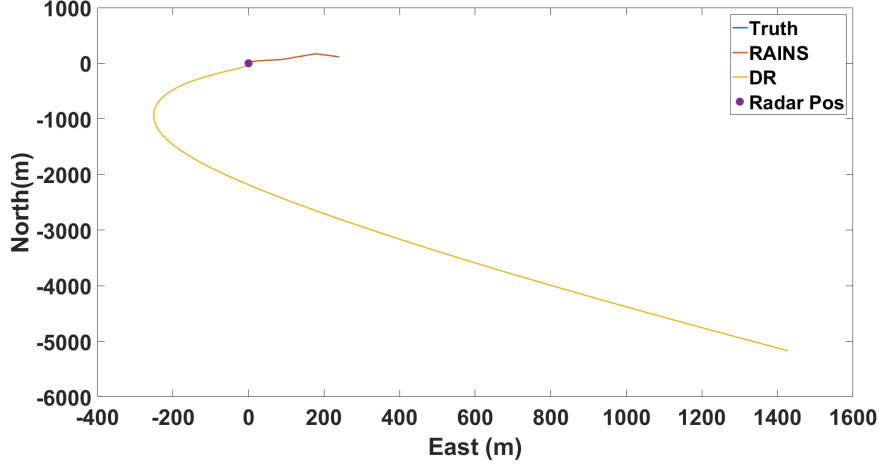Figure 5.6: Simulated Vehicle Heading

Figure 5.7: Simulated Vehicle Position Estimates

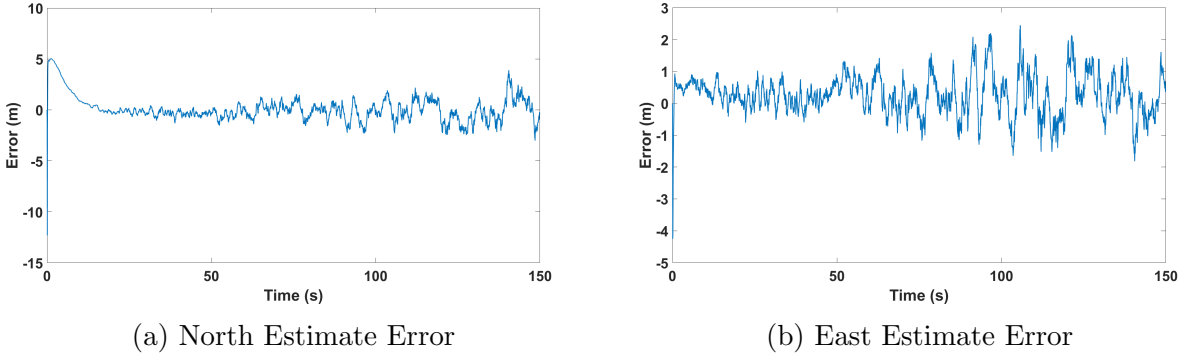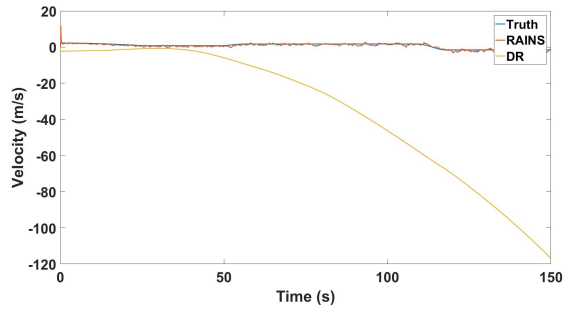(a) North Estimate Error

(b) East Estimate Error

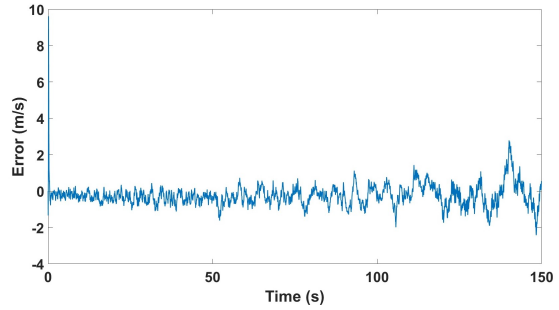Figure 5.8: Position Estimate Error from Simulation

velocity to within two meters per second. Attitude is also accurately estimated, with the RAINS filter reducing the error down to just two degrees, seen in Figures 5.11 - 5.13. One important assumption made in the RAINS filter is that down position and down velocity are zero. Maunally setting these two states to zero raises questions about the observability of the RAINS filter. The concept of observability and its effect on a filter are discussed further in Apendix A.

In theory, the vehicle's position could also be calculated based on range and azimuth measurements using Equations (5.1) and (5.2).

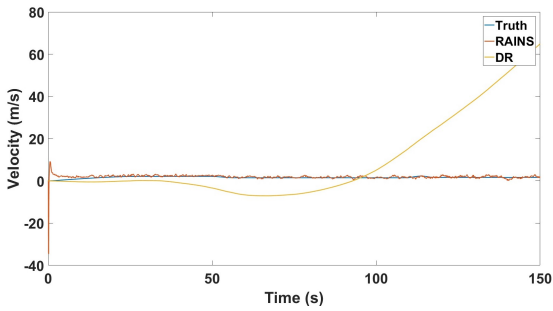$$North = R * \cos \lambda_y \tag{5.1}$$

(a) Velocity North Truth, Estimated, and
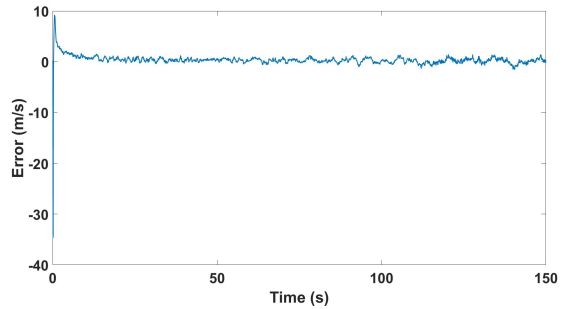Dead-Reckoned

(b) Velocity North Estimate Error

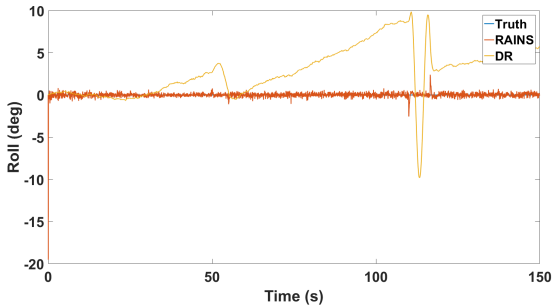Figure 5.9: Velocity North from Simulation

(a) Velocity East Truth, Estimated, and
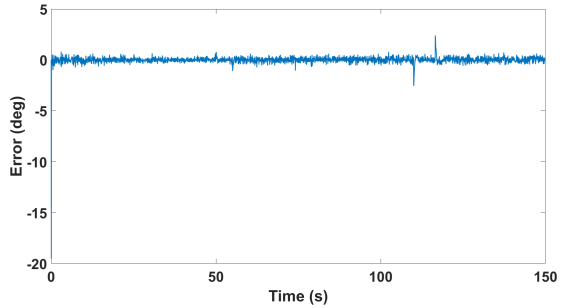Dead-Reckoned

(b) Velocity East Estimate Error
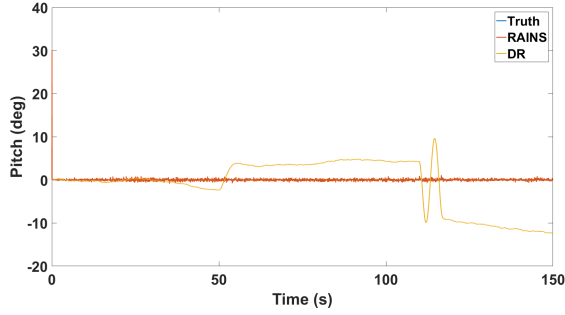
Figure 5.10: Velocity East from Simulation

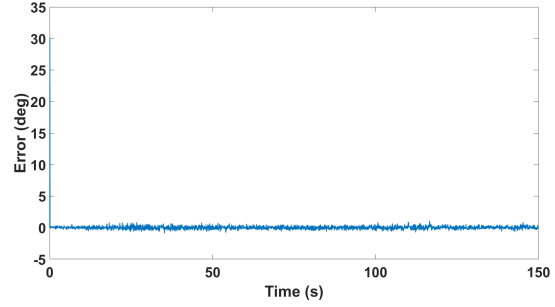(a) Roll Truth, Estimated, and Dead-Reckoned

(b) Roll Estimate Error
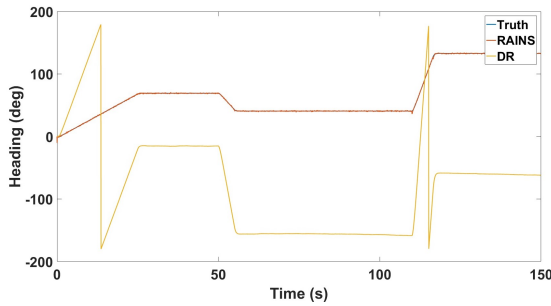
Figure 5.11: Roll from Simulation

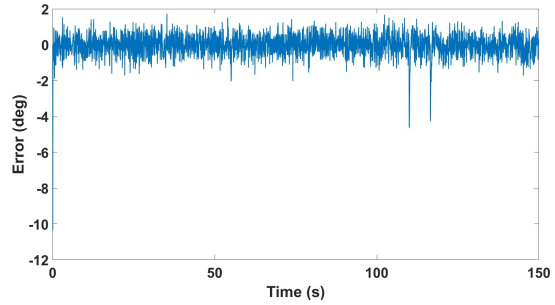(a) Pitch Truth, Estimated, and Dead-Reckoned

(b) Pitch Estimate Error

Figure 5.12: Pitch from Simulation

(a) Heading Truth, Estimated, and
Dead-Reckoned

(b) Heading Estimate Error

Figure 5.13: Heading from Simulation

$$East = R * \sin \lambda_y \tag{5.2}$$

However, radar measurements degrade as distance increases, which can quickly result in large amounts of error. This effect is especially pronounced for the Delphi, which only has a specified maximum effective range between 50-60 meters. Without the filter, the radar alone returns poor position estimates, as shown in Figure 5.14.

5.3 Conclusions

This chapter introduced a new navigation filter called the Radar Aided INS navigation, or the RAINS, filter. It was previously discussed how INS navigation requires additional measurements to accurately estimate a vehicle's position, velocity, and attitude. Although
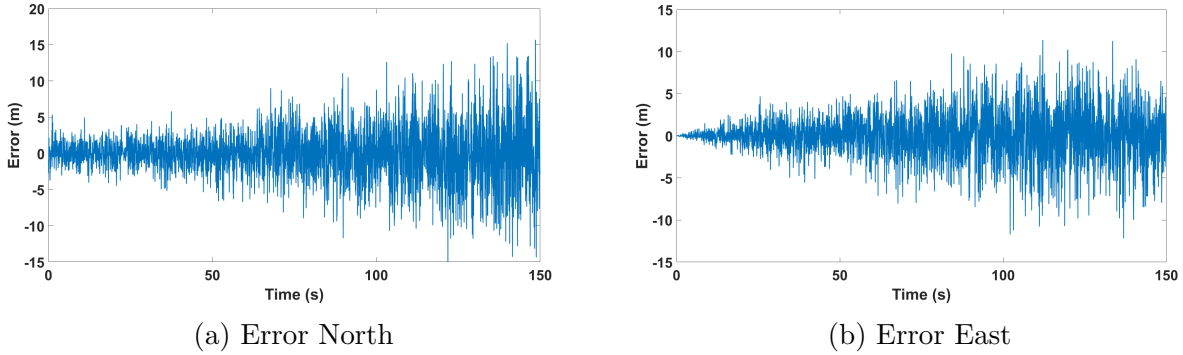
(a) Error North   (b) Error East

Figure 5.14: Error from Radar Calculated Position

GPS is commonly used, it is not always available. To fill the gap when GPS is not available, it was proposed that an INS solution be aided by radar and attitude measurements. By adding these measurement, the estimate uncertainty can be reduced and accurate PVA estimates can be produced.

To verify the RAINS filter, tests were done in simulation. The simulation returned very good results, with position estimates within three meters of truth, velocity within two meters per second, and attitude within two degrees. The sensors simulated for this test were a VectorNav 300 IMU and a Delphi ESR. This simlated test has shown that the filter has potential to overcome the errors caused by INS propagation and constrain the state estimate error covariance.

Chapter 6

Conclusions and Future Work

6.1 Conclusions

Much research has been done regarding navigation and guidance for vehicles, even more so today then ever. The prospect of driverless vehicles requires that highly accurate navigation solutions be available in all circumstances. Although GPS/INS fusion can often meet this need, conditions under which GPS becomes unavailable would prove disastrous as IMUs cannot successfully estimate a vehicle's position, velocity, and attitude over long periods of time without being prohibitively costly. Several topics were addressed in this thesis, culminating in a new filter to fill the gap during GPS outages.

First, magnetometers were introduced. Although magnetometers can suffer from errors such as hard and soft iron bias, once calibrated, they can provide highly accurate heading measurements. The calibration algorithm selected was a batch least-squares estimator that seeks to fit corrupt magnetometer data to an ellipsoid of best fit around the origin. Both simulated data and experimental data was used to demonstrate the effectiveness of this algorithm by showing the magnetometer based heading compared to a reference heading.

When calibrated, magnetometers can also be used for attitude determination when paired with another vector measurement such as acceleration. Although there are many attitude determination algorithms available, for this thesis, an error-minimization least squares estimator that estimates the rotation quaternion was used. Although this algorithm's performance can suffer when a vehicle is undergoing large or sustained accelerations, it was shown to perform well in simulation and with experimental data.

This thesis also analyzed the state estimate error covariance and showed how INS propagation has unbounded uncertainty, while aided INS has bounded uncertainty. The Extended

Kalman Filter was intorduced as a way to incorporate radar and attitude measurements as an aid for INS. Expanding on this idea, a new navigation filter was proposed by this work called the radar-aided INS, or RAINS, filter. The RAINS filter operates by utilizing radar measurement combined with the magnetometer-based attitude measurements to correct the INS propagated estimates. Through simulation, it was shown that the RAINS filter can successfully estimate a vehicle's position, velocity, and attitude.

6.2 Future Work

Although this filter showed that radar and attitude can be used with an IMU to generate position, velocity, and attitude estimates, there is some interesting work that could be done going forward. The magnetometer calibration routine was shown to have issues correctly calibrating the magnetometer in the z-axis, as a vehicle's motion is restricted to a plane. There are algorithms that can calibrate magnetometers real-time, which could potentially lead to higher accuracy in attitude measurement as the magnetometer will be more accurately calibrated in all three axes.

Additionally, the attitude determination algorithm's accuracy suffers under accelerations. One potential option for eliminating this error could be incorporating a vehicle model. The vehicle's acceleration output by the model could be used to remove non-gravitational accelerations. This would make the algorithm a good fit for autonomous vehicles using Model Predictive Control (MPC), as the controller will have a vehicle model and can output the acceleration being commanded so the attitude determination algorithm can make use of it. Besides using a model, the algorithm could also utilize more vector sensors that can increase the accuracy and eliminate singularities under gimbal-lock conditions.

To obtain useable radar measurements, it is necessary to determine the target the radar measurements are coming from. For this thesis, some assumptions were made regarding knowledge about the vehicle's path to acquire the target. Since the main application of this filter would be in an urban canyon, it would makes sense that assumptions such as distance

or range rate of the target could be made. Wherever the radar is located, it would be known how long the road is, so ranges longer than the target road could be removed and range rates higher than the speed limit could also be removed. Although this method of radar data clustering worked for this thesis, there is a potential to get much better measurements without these assumptions. Using statistical target acquisition methods could yield more accurate radar measurements and could even potentially eliminate the errors seen in the position and velocity estimates.

Another method to improve the radar measurements could be implementing better target tracking operations. It is common to use other sensors such as LIDAR to assist radar in target tracking, so there is the opportunity to improve the RAINS filter by using a network of vehicles outfitted with various sensors, including LIDAR [11, 25]. Also, a method of path prediction could be used to assist the radar. By predicting where the vehicle should be and how fast it should be going, measurements that do not match within a certain deviation of these predictions could be thrown out.

Finally, experiemenical verification of the RAINS filter would need to be completed. If the RAINS filter is able to return accurate results with real-world data, it would further validate that the RAINS filter can be used as a navigation tool.

The filter proposed in this thesis opens many opportunities to continue expanding on the concepts of GPS free navigation. The goals of this thesis were to show that INS propagation errors can be bounded with aiding and that radar and attitude measurements can be combined with an IMU to accurately estimate a vehicle's position, velocity, and attitude. These goals were achieved in the form of the RAINS filter and verified in simulation. As computing power continues to increase and the cost of IMUs continue to decrease, it could be possible in the coming years that affordable IMUs may be able to hold a navigation solution without any external aiding. Until that time arrives, they will continue to need innovative ways to improve their navigation abilities. As the push for safe, fully autonomous vehicles

grows, these innovations will continue, bringing about ever increasing accuracy in guidance and navigation for everyone.

Bibliography

[1] Allard,Dean C. The Development of the Radio Proximity Fuze. Johns Hopkins APL Technical Digest, vol 3. pp. 358-59.

[2] Alonso, Roberto, and Malcolm D. Shuster. TWOSTEP: A Fast Robust Algorithm for Attitude-Independent Magnetometer-Bias Determination. The Journal of the Astronautical Sciences, vol. 50, no. 4, Dec. 2002, pp. 433-451.

[3] Alonso, Roberto, and Malcolm D. Shuster. Complete Linear Attitude-Independent Magnetometer Calibration. The Journal of the Astronautical Sciences, vol. 50, no. 4, Dec. 2002, pp. 477-490.

[4] Alonso, Roberto, and Malcolm D. Shuster. Attitude-Independent Magnetometer-Bias Determination: A Survey. The Journal of the Astronautical Sciences, vol. 50, no. 4, Dec. 2002, pp. 453-475.

[5] Bak, T. Spacecraft Attitude Determination - A Magnetometer Approach. Aalborg University, 1999.

[6] Bar-Shalom, Yaakov, et al. The Probabilistic Data Association Filter. IEEE Control Systems Magazine, vol. 29, no. 6, Dec. 2009, pp. 82–100.

[7] By Britannica. https://www.britannica.com/technology/radar/Introduction

[8] Buderi, Robert. The Invention That Changed the World: How a Small Group of Radar Pioneers Won the Second World War and Launched a Technical Revolution. Simon and Schuster, 1998.

[9] Caruso, M. J. Applications of Magnetic Sensors for Low Cost Compass Systems. Position Location and Navigation Symposium. IEEE, 2000, pp. 177-184.

[10] Caruso, Michael J. Applications of Magnetoresistive Sensors in Navigation Systems. SAE International Congress and Exposition. 1997.

[11] Cho, Hyunggi, et al. A multi-sensor fusion system for moving object detection and tracking in urban driving environments. Robotics and Automation (ICRA), 2014 IEEE International Conference on. IEEE, 2014.

[12] Choi, Charles Q. Magma Ocean Could Have Given Early Earth Magnetic Field. 6 Dec. 2013, https://www.livescience.com/41758-earth-magnetic-field-magma-ocean.html.

[13] Cobb, Susan. Weather Radar Development Highlight of the National Severe Storms Laboratory First 40 Years. NOAA Magazine, 2009.

[14] Davenport, Paul B. A Vector Approach to the Algebra of Rotations with Applications. NASA Technical Note, 1968.

[15] Diebel, James. Representing Attitude: Euler Angles, Unit Quaternions, and Rotation Vectors. Stanford University, 20 Oct. 2006.

[16] Gebre-Egziabher, Demoz. Magnetometer Autocalibration Leveraging Measurement Locus Constraints. Journal of Aircraft, vol. 44, no. 4, July 2007, pp. 1361-1368.

[17] Gebre-Egziabher, D., and G. H. Elkaim. MAV Attitude Determination by Vector Matching. IEEE Transactions on Aerospace and Electronic Systems, vol. 44, no. 3, July 2008, pp. 1012-1028.

[18] Gebre-Egziabher, Demoz, et al. Calibration of Strapdown Magnetometers in Magnetic Field Domain. Journal of Aerospace Engineering, vol. 19, no. 2, Apr. 2006, pp. 87-102.

[19] Felch, E. P., et al. Air-Borne Magnetometers for Search and Survey. Transactions of the American Institute of Electrical Engineers, vol. 66, no. 1, Jan. 1947, pp. 641-651.

[20] Gautier, Jennifer D. GPS/INS Generalized Evaluation Tool (GIGET) for the Design and Testing of Integrated Navigation Systems. Stanford University, June 2003.

[21] Groves, Paul D. Principles of GNSS, Inertial, and Multisensor Integrated Navigation Systems. 2nd ed, Artech House, 2013.

[22] Golding, A. R., and N. Lesh. Indoor Navigation Using a Diverse Set of Cheap, Wearable Sensors. IEEE Comput. Soc, 1999, pp. 29?36.

[23] Huurdeman, Anton A. The Worldwide History of Telecommunications. Wiley, 2003.

[24] International Geomagnetic Reference Field. 22 Dec. 2014, https://www.ngdc.noaa.gov/IAGA/vmod/igrf.html.

[25] Kato, Takeo, Yoshiki Ninomiya, and Ichiro Masaki. An obstacle detection method by fusion of radar and motion stereo. IEEE Transactions on Intelligent Transportation Systems 3.3 (2002). pp. 182-188.

[26] Katz, Victor J. A History of Mathematics, Brief Version. Addison-Wesley, 2004.

[27] Kim, Jinwhan, et al. Comparison Between Three Spiraling Ballistic Missile State Estimators. American Institute of Aeronautics and Astronautics, 2008.

[28] Wonmo Koo, et al. Error Calibration of Magnetometer Using Nonlinear Integrated Filter Model With Inertial Sensors. IEEE Transactions on Magnetics, vol. 45, no. 6, June 2009, pp. 2740-2743.

[29] Lowrie, William. Fundamentals of Geophysics. Cambridge University Press, 2007.

[30] Kwanmuang, Surat, et al. Magnetometer-Enhanced Personal Locator for Tunnels and GPS-Denied Outdoor Environments. Unmanned, Robotic, and layered Systems, April 25-29, 2011.

[31] Marins, J. L., et al. An Extended Kalman Filter for Quaternion-Based Orientation Estimation Using MARG Sensors. International Conference of Intelligent Robots and Systems. Vol. 4, IEEE, 2001, pp. 2003-2011.

[32] Marins, J. L., et al. An Extended Kalman Filter for Quaternion-Based Orientation Estimation Using MARG Sensors. Vol. 4, IEEE, 2001, pp. 2003?11.

[33] Martin, Scott. Closely Coupled GPS/INS Relative Positioning for Automated Vehicle Convoys. Auburn University, 9 May 2011.

[34] By MathsPoetry - Own work (Personal drawing), CC BY-SA 3.0, https://commons.wikimedia.org/w/index.php?curid=5948979

[35] By MathsPoetry - Own work, CC BY-SA 3.0, https://commons.wikimedia.org/w/index.php?curid=5949077

[36] Morales, Gabriel. Magnetometer Aided Navigation Filters ForImproved Observability and Estimation on Ground Vehicles. Auburn University, August 2016.

[37] Mortari, Daniele. ESOQ: A Closed-Form Solution to the Wahba Problem. Journal of Astronautical Sciences, vol. 45.2, 1997, pp. 195-204.

[38] Ornedo, R. S., et al. GPS and Radar Aided Inertial Navigation System for Missile System Applications. IEEE, 1998, pp. 614–21.

[39] Pierce, Daniel. Incorporation of a Foot-Mounted IMU for Multi-Sensor Pedestrian Navigation. Auburn University, 7 May 2016.

[40] Roumeliotis, Stergios I., Sukhatme, Gaurav S., Bekey, George A. Circumventing Dynamic Modeling: Evaluation of the Error-State Kalman Filter Applied to Mobile Robot Localization. International Conference of Robotics and Automation. Vol. 4, IEEE, 1999, pp. 1656-1664.

[41] Ryan, Jonathan. A Fully Integrated Sensor Fusion Method Combining a Single Antenna GPS Unit with Electronic Stability Control Sensors. Auburn University, 6 Aug. 2011.

[42] Schokley, Jeremiah A. Ground Vehicle Navigation Using Magnetic Field Variation. Air Force Institute of Technology, Sept. 2012.

[43] Sherer, Tyler. Radar Probabilistic Data Association Filter with GPS Aiding for Target Selection and Relative Position Determination. Auburn University, 6 May 2017.

[44] Shuster, M. D., and S. D. Oh. Three-Axis Attitude Determination from Vector Observations. Journal of Guidance, Control, and Dynamics, vol. 4, no. 1, Jan. 1981, pp. 70-77.

[45] Sidi, Marcel J. Spacecraft Dynamics and Control: A Practical Engineering Approach. Cambridge Univ. Press, 1997.

[46] Skolnik, Merrill I., editor. Radar Handbook. 3rd ed, McGraw-Hill, 2008.

[47] Soken, H. E., and Sakai, S. Magnetometer only attitude estimation for spinning small satellites. Recent Advances in Space Technologies. Istanbul, Turkey, 2017. pp. 369-374.

[48] Valenti, Roberto, et al. Keeping a Good Attitude: A Quaternion-Based Orientation Filter for IMUs and MARGs. Sensors, vol. 15, no. 8, Aug. 2015, pp. 19302–30.

[49] Wahba, Grace. A Least Squares Estimate of Satellite Attitude. SIAM Review, vol. 7, no. 3, July 1965, pp. 409-409.

[50] Watson, Raymond C. Radar Origins Worldwide: History of Its Evolution in 13 Nations through World War II. Trafford Publ, 2009.

[51] Xu, Jiahe, Dimirovski, Georgi M. UKF Design and Stability for Nonlinear Stochastic Systems with Correlate Noises. IEEE, 2007. pp. 6226-6231.

Appendices

Appendix A

Oberservability of the RAINS Filter

An important indicator on the performance of a filter is the filter's observability. Observability is a measure of how well a filter can estimate its states. To determine a filter's observability, the rank of the observability matrix must be taken. Ideally, the observability matrix would be full rank. A full rank observability matrix indicates that all states can be observed and estimated given the dynamics of the system and the measurements being taken. However, full rank is not a requirement in state estimation, as the commonly used closesly-coupled GPS-INS coupled filters have 17 states, but commonly only have a rank of 14 [36]. In a discrete time system, the observability matrix can be calculated by the following equation.

$$O_{LTV}(t_f, t_0) = \int_{t_0}^{t_f} F^T(\tau, t_0) H^T H F(\tau, t_0) d\tau \tag{A.1}$$

$F^T(\tau, t_0)$ is the state transition matrix at the current time step, and H is the measurement Jacobian. $O_{LTV}(t_f, t_0)$ is the observability grammian, evaluated from t_0 to t_f. The observability of a system is indicated if the grammian is non-singular, which can be determined by taking the rank of O_{LTV}.

A.1   RAINS Filter Observability

To test the observability of the RAINS filter, an observability analysis was performed. Looking at the results in Figure A.1, the observabilty matrix only reaches a rank of 8. This means that almost half of the 15 states are unable to be observed, which greatly reduces confidence in the estimates of the filter.
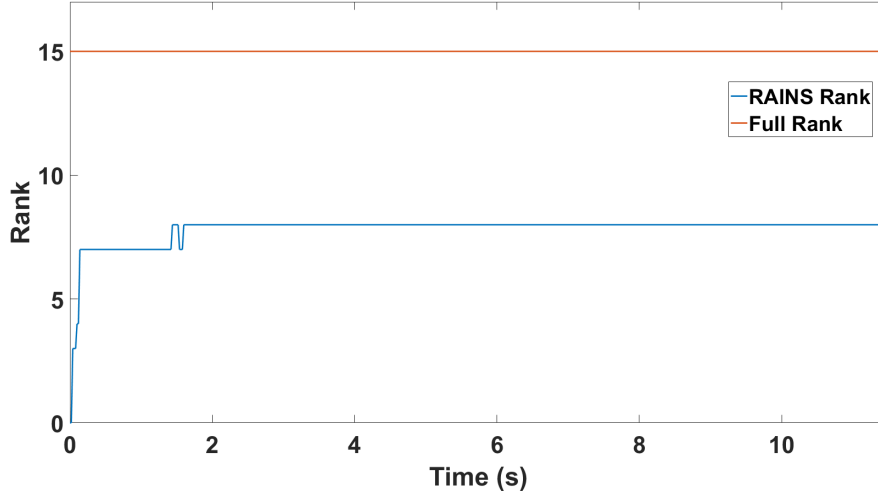
Figure A.1: RAINS Filter Observability

Since the rank of the observability matrix is so low, it indicates that there would be several states that are not being estimated. After some investigation, it was determined that the bias states were not being estimated, and instead trended to zero. Since bias is not estimated, there was potential to improve the RAINS filter by removing the bias estimates.

Removing the bias estimates is a decision about managing tradeoffs in filter performance. In GPS-INS filters, the bias is estimated so that PVA solutions could still be generated in brief periods where GPS may not be available. If the bias is not estimated in the RAINS filter, then the filter permance would greatly suffer without the radar measurements. It was decided that removing the bias estimates would not be an issue, because this filter is not inteded to be used in situations where radar would be intermittent. It is assumed the vehicle will always be in the radar's line of sight.

The Delphi also has the limitation of not being able to measure elevation. This causes down and down velocity to be onobservable. In previous cases, these states were manually set to zero. However, this can cause errors in the covariance matrix, P. To correct this in the observability analysis, the down and down velocity states were also removed.

A.2 Reduced State RAINS Filter

If bias, down, and down velocity are no longer being estimated, the structure of the RAINS filter must be changed. This results in a similar filter structure, but with reduced states. The propagation model will no longer have the bias estimates involved as follows

$$\hat{R}_{b,k+1}^n = \hat{R}_{b,k}^n (I_{33} + \Omega_{ib} dt) \tag{A.2}$$

$$\Omega_{ib} = [(\omega_k] \tag{A.3}$$

$$f_{ib}^n = \frac{1}{2}(\hat{R}_{b,k+1}^n + \hat{R}_{b,k}^n)(\alpha_k) \tag{A.4}$$

$$\hat{V}_{k+1} = \hat{V}_k + (f_{ib}^n + g_n)\Delta t \tag{A.5}$$

$$\hat{P}_{k+1} = \hat{P}_k + \frac{\Delta t}{2}(\hat{V}_{k+1} + \hat{V}_k) \tag{A.6}$$

The state vector will similarly have the bias removed.

$$\hat{x} = \begin{bmatrix} \delta N & \delta E & \delta \dot{N} & \delta \dot{E} & \delta \phi & \delta \theta & \delta \psi \end{bmatrix}^T \tag{A.7}$$

Since the state vector has been reduced, the system dynamics model matrix, process noise covariance matrix, and system model noise sources matrix will all be reduced.

$$F = \begin{bmatrix} O_{22} & I_{22} & O_{23} \\ O_{22} & O_{22} & [(R_{b,red}^n \underline{\alpha})\wedge] \\ O_{32} & O_{32} & O_{33} \end{bmatrix} \tag{A.8}$$

$$Q = \begin{bmatrix} \sigma_a^2 & 0_{33} \\ 0_{33} & \sigma_g^2 \end{bmatrix} \tag{A.9}$$

65

$$B_w = \begin{bmatrix} 0_{23} & 0_{23} \\ R^e_{b,red} & 0_{23} \\ 0_{33} & R^e_b \end{bmatrix} \qquad (A.10)$$

A subscript of *red* indicates a reduced rotation matrix that only includes the first and second rows. The third row is no longer needed in the cases where it would produce a down or down velocity. The measurement matrix, H, is also reduced to account for the removed states.

$$H_1 = \begin{bmatrix} \frac{-Y}{X^2+Y^2} \\ \frac{X}{X^2+Y^2} \\ 0_{5,1} \end{bmatrix}^T \qquad (A.11)$$

$$H_2 = \begin{bmatrix} \frac{X}{\sqrt{X^2+Y^2+Z^2}} \\ \frac{Y}{\sqrt{X^2+Y^2+Z^2}} \\ 0_{5,1} \end{bmatrix}^T \qquad (A.12)$$

$$H_3 = \begin{bmatrix} \frac{\dot{X}}{\sqrt{X^2+Y^2+Z^2}} - \frac{X(X\dot{X}+Y\dot{Y}+Z\dot{Z})}{(X^2+Y^2+Z^2)^{3/2}} \\ \frac{\dot{Y}}{\sqrt{X^2+Y^2+Z^2}} - \frac{Y(X\dot{X}+Y\dot{Y}+Z\dot{Z})}{(X^2+Y^2+Z^2)^{3/2}} \\ \frac{X}{\sqrt{X^2+Y^2+Z^2}} \\ \frac{Y}{\sqrt{X^2+Y^2+Z^2}} \\ 0_{3,1} \end{bmatrix}^T \qquad (A.13)$$

$$H_4 = \begin{bmatrix} 0_{32} \\ 0_{32} \\ I_{33} \end{bmatrix}^T \qquad (A.14)$$

H will still be matrix composed of the above vectors.

$$H = \begin{bmatrix} H_1 \\ H_2 \\ H_3 \\ H_4 \end{bmatrix} \tag{A.15}$$

A.3   Reduced-State Simulation Results

To test this reduced state filter, the simulated data shown in Figures A.2 - A.4 was passed through the new, reduced-state filter.
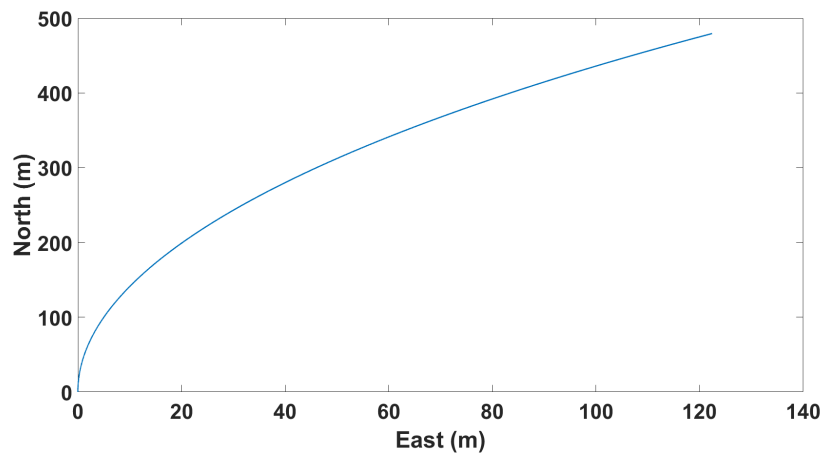
Figure A.2: Simulated Vehicle Trajectory
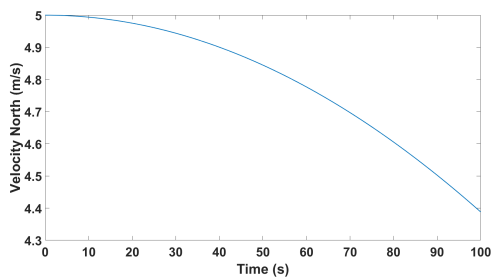
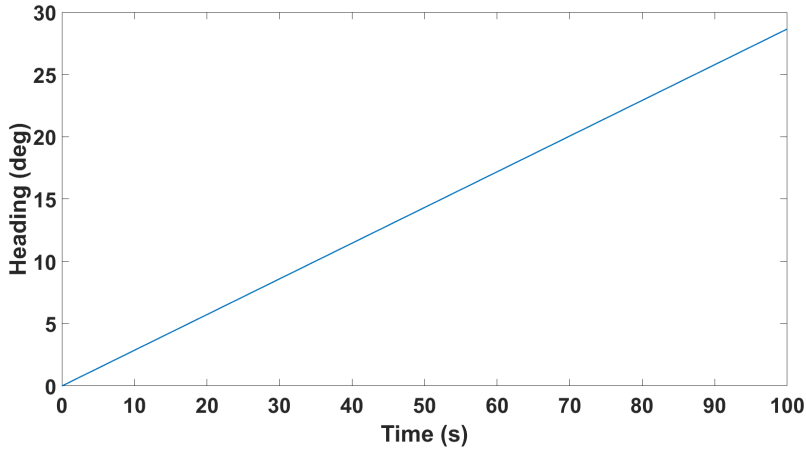(a) North Velocity
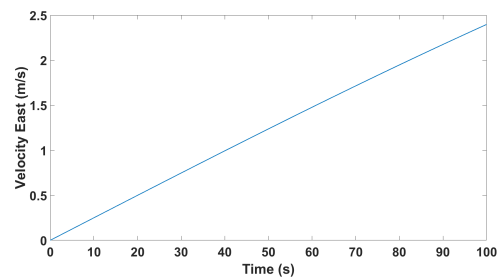
(b) East Velocity

Figure A.3: Simulated Vehicle Velocity

Figure A.4: Simulated Vehicle Heading

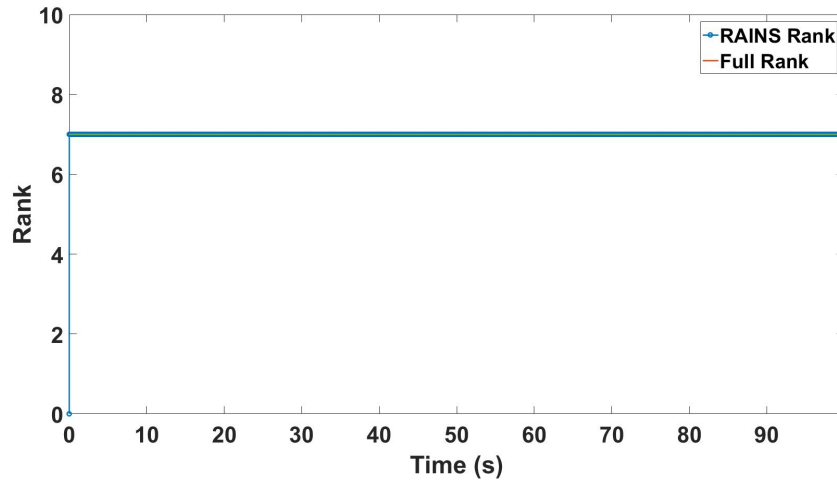The rank of the observability matrix with this simulated data is shown in Figure A.5.

Figure A.5: Rank of Observability Matris with No Bias, Down, or Down Velocity Estimates

The rank of this new filter is seven, which is now full rank after all other states have been removed. Position estimates, shown in Figure A.6, are within five meters of truth. Velocity estimates, shown in Figure A.7, are good, staying at less than two meters per second. Attitude estimates, in Figure A.8, remain similar to before the states were removed. Despite initialization errors, all attitude estimate errors converge towards zero with noise error of approximately two degrees.
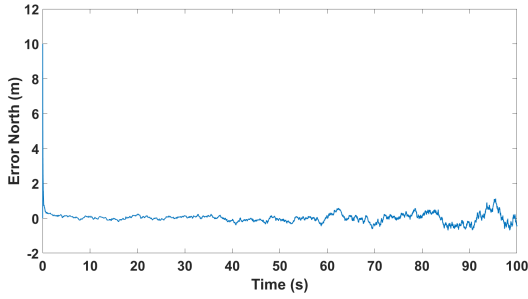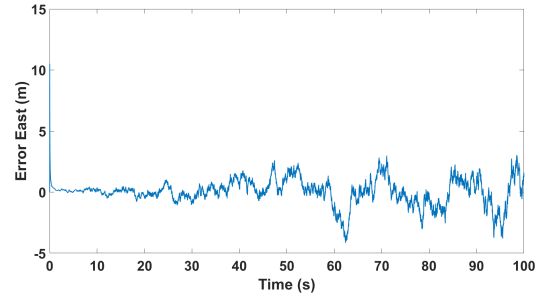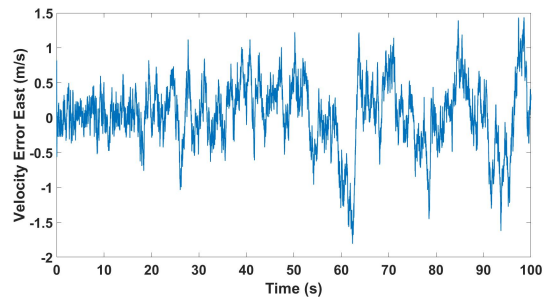
(a) Error North
(b) Error East

Figure A.6: Estimator Position Error
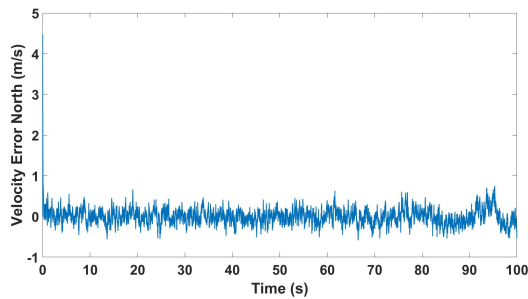

(a) Error North
(b) Error East

Figure A.7: Estimator Velocity Error

A.4   Conclusions

Observability is an important indicator on the trustworthiness of a filter's estimates. A rank-deficient observability matrix could indicate a potential for instability or erroneous estimates. By removing the bias and down estimates in the RAINS filter, the potential for instability has been removed. Although this means the filter cannot operate without radar measurements for an extended period of time, the tradeoff would be worth it for the confidence that all states are being estimated accurately.
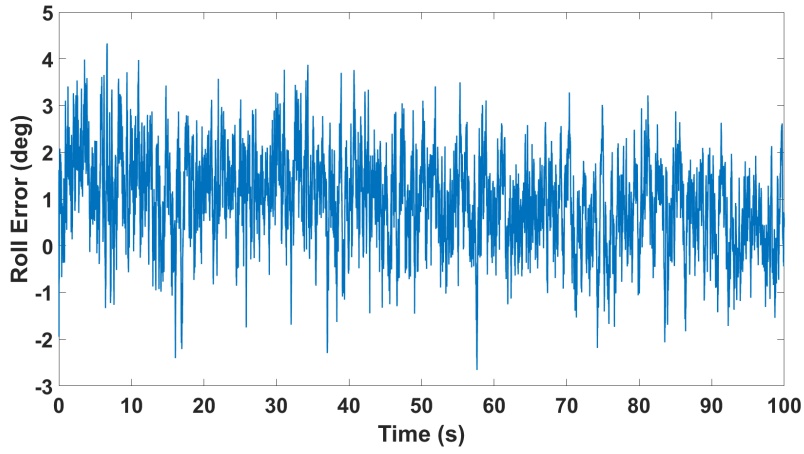
(a) Roll Estimate Error
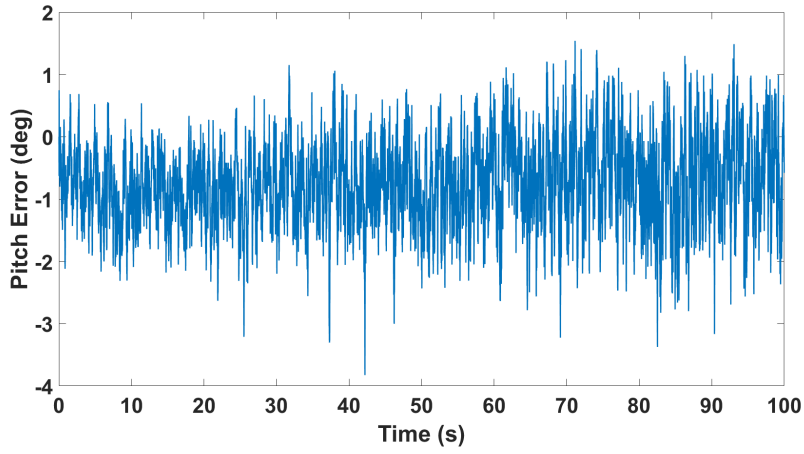
(b) Pitch Estimate Error
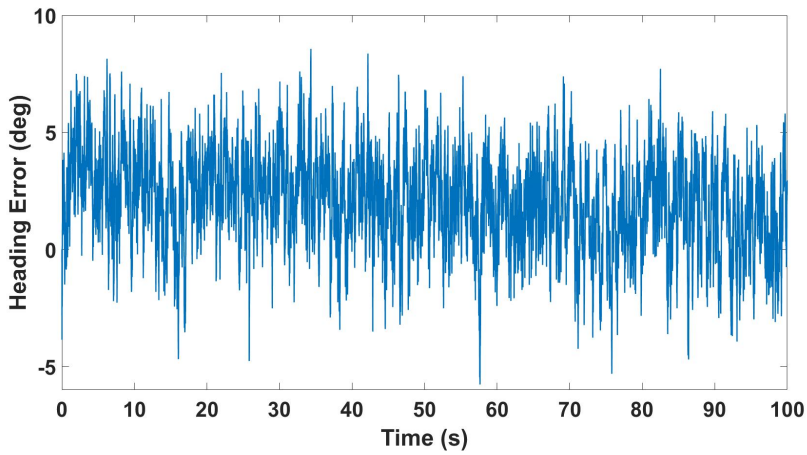
(c) Heading Estimate Error

Figure A.8: Attitude Estimate Errors

Appendix B

RAINS Filter and Correlated Noise

One major drawback to the RAINS filter lies in how the acceleromter measurementes are used. The measurements are first used to propagate the states in the time update through IMU propagation, and then again indirectly through the AHRS in the measurement update. One of the fundamental assumptions of the Kalman Filter is that the Process Noise (Q), and Measurement Noise (R) covariance matrices are uncorrelated. However, since the RAINS filter used the acceleromter measurement in the time and measurement update, this causes the Q and R matrices to become correlated. To test the validity of the RAINS filter in light of this fact, a centralized filter that decorrelates the process noise and measurement noise covariance matrices was tested to see if navigation estimates could be improved.

B.1   Centralized Filter Formulation

The centralized fitler decorrelates the Q and R matrices by expanding the state vector to include body-frame acceleration and angular rate measurement estimate errors. This produces the following state vector

$$\hat{x} = \begin{bmatrix} \delta P & \delta V & \delta\alpha_{xyz} & \delta\Psi & \delta\dot{\Psi}_{xyz} & b_a & b_g \end{bmatrix}^T \tag{B.1}$$

where $\delta\alpha_{xyz}$ are the estimated accelerations in the vehicle body frame and $\delta\dot{\Psi}_{xyz}$ are the estimated body frame angular rates. The propagation equations will now use the estimated acceleration and angular rates instead of the measured acceleration and angular rates.

$$\hat{R}^n_{b,k+1} = \hat{R}^n_{b,k}(I_{33} + \Omega_{ib}dt) \tag{B.2}$$

$$\Omega_{ib} = [\dot{\hat{\Psi}}_{xyz,k}] \tag{B.3}$$

$$f_{ib}^n = \hat{\alpha}_{xyz,k} \tag{B.4}$$

$$\hat{V}_{k+1} = \hat{V}_k + (f_{ib}^n + g_n)\Delta t \tag{B.5}$$

$$\hat{P}_{k+1} = \hat{P}_k + \frac{\Delta t}{2}(\hat{V}_{k+1} + \hat{V}_k) \tag{B.6}$$

$$\dot{\hat{\Psi}}_{xyz,k+1} = \dot{\hat{\Psi}}_{xyz,k} \tag{B.7}$$

These equations will yield the following system dynamics model, F.

$$F = \begin{bmatrix} O_{33} & I_{33} & O_{33} & O_{33} & O_{33} & O_{33} & O_{33} \\ O_{33} & O_{33} & R_b^n & [(R_b^n\underline{\alpha})\wedge] & O_{33} & R_b^n & O_{33} \\ O_33 & O_{33} & O_{33} & O_{33} & O_{33} & O_{33} & O_{33} \\ O_{33} & O_{33} & O_{33} & O_{33} & O_{33} & O_{33} & R_b^n \\ O_{33} & O_{33} & O_{33} & O_{33} & O_{33} & O_{33} & O_{33} \\ O_{33} & O_{33} & O_{33} & O_{33} & O_{33} & -\frac{1}{\tau_a}I_{33} & O_{33} \\ O_{33} & O_{33} & O_{33} & O_{33} & O_{33} & O_{33} & -\frac{1}{\tau_g}I_{33} \end{bmatrix} \tag{B.8}$$

In the centrazlied filter, the driving input is white noise on jerk and angular acceleration, which will result in Q and B_w matrices of the following form

$$Q = \begin{bmatrix} \sigma_j^2 & 0_{33} & 0_{33} & 0_{33} \\ 0_{33} & \sigma_{\dot{\Psi}}^2 & 0_{33} & 0_{33} \\ 0_{33} & 0_{33} & \sigma_{ba}^2 & 0_{33} \\ 0_{33} & 0_{33} & 0_{33} & \sigma_{bg}^2 \end{bmatrix} \tag{B.9}$$

$$B_w = \begin{bmatrix} 0_{33} & 0_{33} & 0_{33} & 0_{33} \\ 0_{33} & 0_{33} & 0_{33} & 0_{33} \\ I_{33} & 0_{33} & 0_{33} & 0_{33} \\ 0_{33} & 0_{33} & 0_{33} & 0_{33} \\ 0_{33} & I_{33} & 0_{33} & 0_{33} \\ 0_{33} & 0_{33} & I_{33} & 0_{33} \\ 0_{33} & 0_{33} & 0_{33} & I_{33} \end{bmatrix} \tag{B.10}$$

where the new terms in the Q matrix, σ_j^2 and $\sigma_{\dot\Psi}^2$ represent the variances on jerk and angular acceleration. Since there is no direct way to quantify the variances on these two variables, they are purely a tuning parameter. A good starting to point is to use the variances for the acceleromter and gyroscope, and tune it until desired results are achieved. The measurement vector in the centralized filter is also expanded, shown in Equation (B.11).

$$z = \begin{bmatrix} \lambda_y & R & \dot{R} & \alpha_{NED} & \tilde{\dot{\Psi}}_{xyz} & \tilde{\alpha}_{xyz} & \Psi \end{bmatrix}^T \tag{B.11}$$

The additional measurements now include the navigation frame acceleration, α_{NED}, the gyroscope measurements $\tilde{\dot{\Psi}}_{xyz}$, and the acclerometer measurements $\tilde{\alpha}_{xyz}$, along with the three radar measurements λ_y, R, and $\dot{R}$, and the attitude meausurements Ψ. In the centralized filter, the attitude measurements are now found by using magnetometer measurements and the estimated body frame acceleration, as opposed to the actual accelermeter measurements. The equations defining the new measurements used in the centralized filter can be written as follows

$$\alpha_{NED} = R_{b,k+1}^n \hat{\alpha}_{xyz,k} \tag{B.12}$$

$$\tilde{\dot{\Psi}}_{xyz} = \tilde{\dot{\Psi}}_{xyz} - \hat{b}_{g,k} \tag{B.13}$$

$$\tilde{\alpha}_{xyz} = \tilde{\alpha}_{xyz} - \hat{b}_{a,k} \tag{B.14}$$

where m_e is the IGRF model of earth's magnetic field. These new measurement can be added to the measurement matrix by once again taking the partial derivates of each equation with respect to the states. The partial derivates for α_{NED} and $\tilde{m}_{xyz}$ result in long, complex equation because of the presence of the rotation matrices.

B.2 Simulation Results of the Centralized Filter

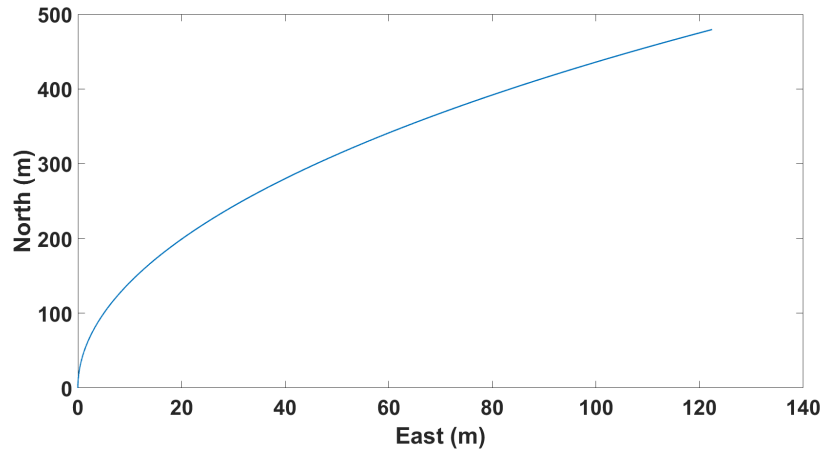The centralized filter was tested in simulation with trajectory shown in Figures B.1 - B.3.

Figure B.1: Simulated Vehicle Trajectory

(a) North Velocity

(b) East Velocity
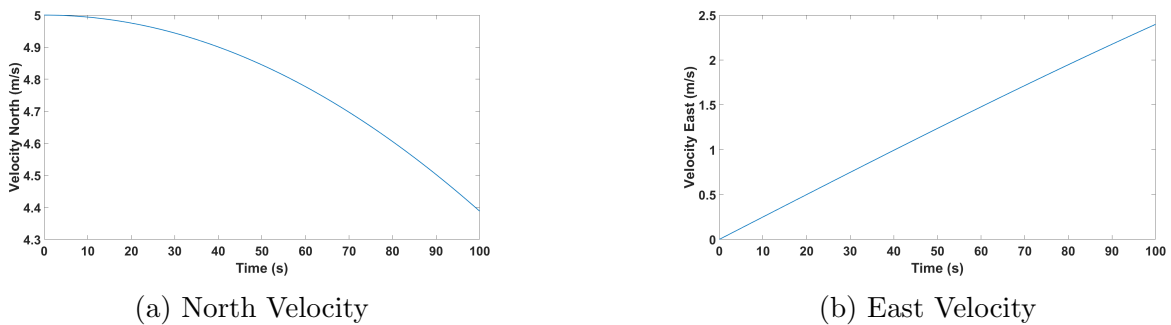
Figure B.2: Simulated Vehicle Velocity

The position estimate errors, shown in Figure B.4, have results that are similar to the RAINS filter, within about three meters or less of truth.
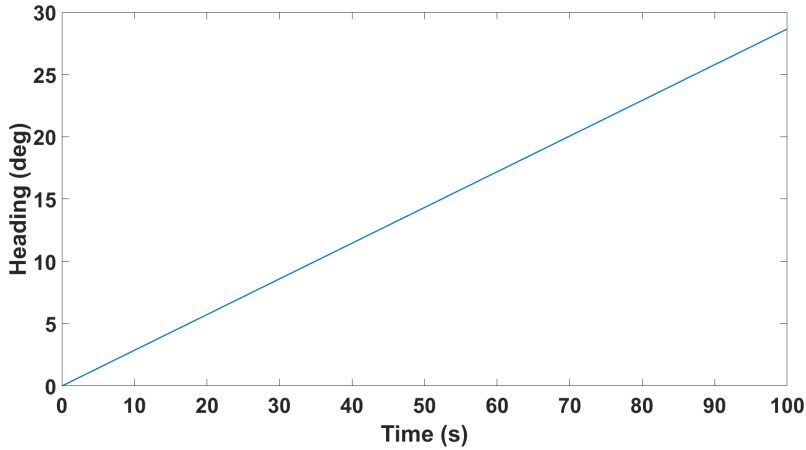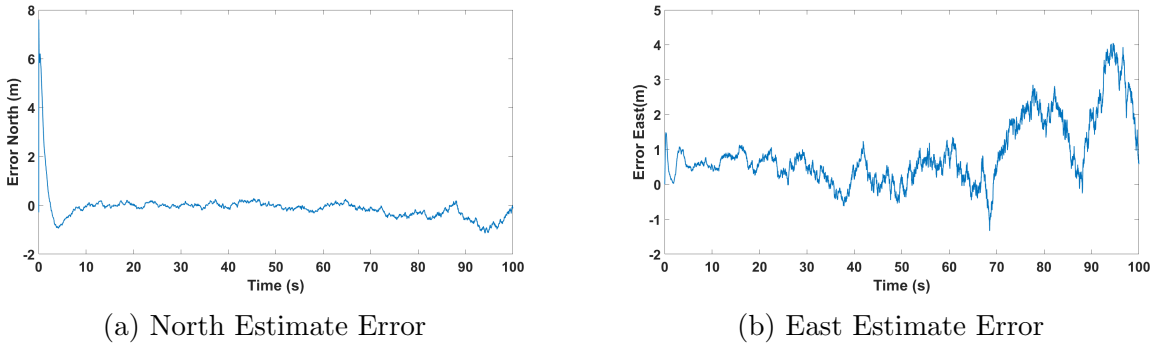
Figure B.3: Simulated Vehicle Heading
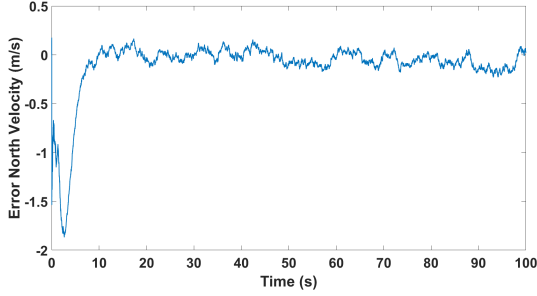

(a) North Estimate Error

(b) East Estimate Error

Figure B.4: Simulated Position Estimate Error

Velocity estimate errors, shown in Figure B.5, are also similar to the RAINS filter. The error stays within two meters per second of truth. Attitude estaimtes, shown in Figure B.6, once again match closely with the RAINS filter and stay within two degrees of truth.

B.3   Conclusions

The results of the centralized filter match closely with the results of the RAINS filter. This shows that the RAINS filter is still a valid option for estimation despite the correlated noise. These results are not totally unexpected, even if they do violate an assumption of the Kalman Filter. There has been other work done involving Extended Kalman Filters with correlated noise that show EKFs can still operate with high accuracy even with the process

(a) North Velocity Estimate Error
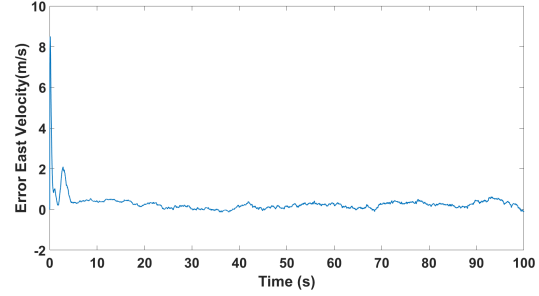
(b) East Velocity Estimate Error

Figure B.5: Simulated Velocity North

noise and measurement noise matrices being correlated [36,51]. Even though the centralized filter avoids the correlated noise issue altogether, it has one major drawback that prevents it from becoming a preferrable option over the RAINS filter. To illustrate this drawback, observe the equation for calculating the Kalman gain matrix in Equation B.15.

$$L_{k+1} = P^-_{k+1} H^T_{k+1} (H_{k+1} P^-_{k+1} H^T_{k+1} + R)^{-1} \tag{B.15}$$

Calculating the Kalman gain matrix requires taking the inverse of a matrix of the same dimension as R. In the centralized filter, the m number of measurements has increased from six to 15, while the n number of states being estimated increases from 15 to 21. According to [21], calculating the matrix inverse of the Kalman Gain requires $\frac{3}{2}m^3 - \frac{1}{2}m$ number of multiplications and approximately m^3 number of additions. This causes the centralized filter to be drastically slower than the RAINS filter, and would greatly increase the computation requirements and difficulty of real-time implementation. For this reason, the RAINS filter remained the estimate method of choice in this thesis.
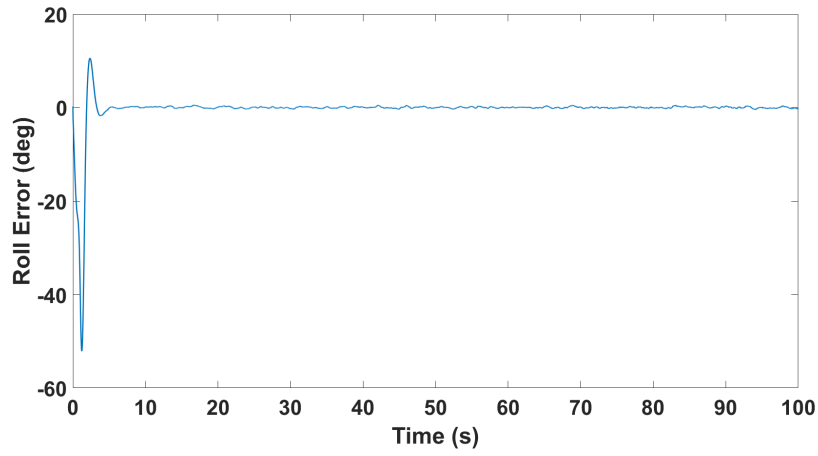
(a) Roll Estimate Error
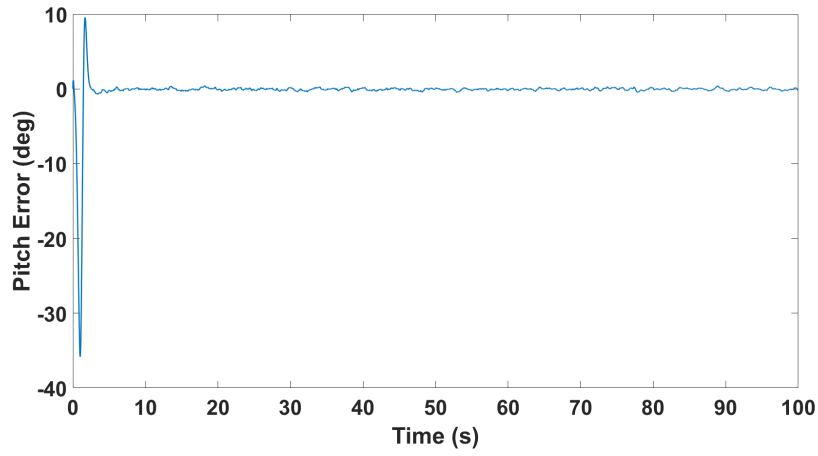
(b) Pitch Estimate Error
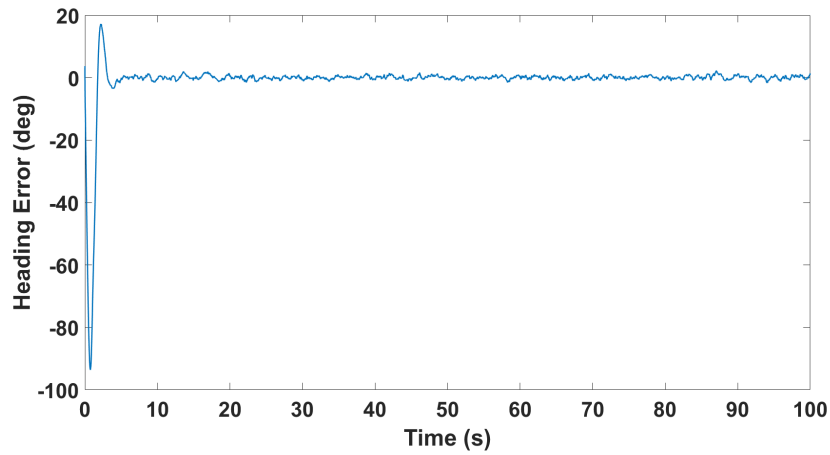
(c) Heading Estimate Error

Figure B.6: Attitude Estimate Errors